ACS OMEGA

http://pubs.acs.org/journal/acsodf

Article

Hydrodynamic Analysis and Cake Erosion Properties of a Modified Water-Based Drilling Fluid by a Polyacrylamide/Silica Nanocomposite during Rotating-Disk Dynamic Filtration

Hamed Movahedi, Saeid Jamshidi,* and Mastaneh Hajipour

Cite This: *ACS Omega* 2022, 7, 44223−44240

Read Online

ACCESS | Metrics & More | Article Recommendations

ABSTRACT: In this study, the potential of using a polyacrylamide-silica nanocomposite (PAM-S) to control the filtration properties of bentonite water-based drilling muds under different salinity conditions was evaluated. Static filtration tests under low-pressure/low-temperature (LPLT) conditions accompanied by rheological measurements have been carried out to analyze the role of silica nanoparticles (NPs) and nanocomposites (NCs) in the base fluid properties. Moreover, high-pressure/high-temperature (HPHT) static filtration was also investigated to evaluate the thermal stability of PAM-S. Afterward, dynamic filtration has been conducted in a filtration cell equipped with an agitating system with a disk-type impeller to investigate the hydrodynamic and formation of a filter cake under shear flow conditions. Fluid flow velocity and wall shear stress (WSS) distribution over the filter cake were analyzed using an exact 3D computational fluid dynamic (CFD) simulation. A transparent filtration cell with a camera was used to accurately record the fluid flow field inside the filter press and validate the CFD results. The obtained results indicated that adding silica NPs at a concentration of less than 2 wt % increases the fluid loss due to reducing rheological properties such as yield point. While silica NPs could not significantly change the mud properties, the experimental results showed that, under both LPLT and HPHT conditions, the PAM-S NC could reduce the total filtration loss by 70% at a low concentration of 0.75 wt %. Moreover, during dynamic filtration, the results indicated that there is a linear relationship between the cake thickness and the inverse of WSS at different operating pressures. However, no correlation could be found between predeposited mud cake erosion and WSS. At a rotating disk speed of 1000 rpm, more than 60% of the predeposited mud cake was eroded after 30 min for a saline mud sample while for the NC-treated mud sample cake erosion is considerably reduced and reaches up to 20% at 1.5 wt % PAM-S.

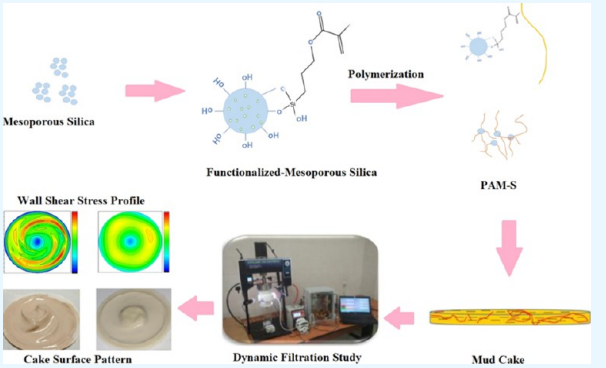

1. INTRODUCTION

The drilling fluid circulation system is one of the critical parts of drilling oil and gas wells. Drilling mud has various roles, such as cooling the drill bit and drill string, hole cleaning or transporting the drilling cuttings to the surface, stabilizing the wellbore, and proper filtration.[1−5] Various drilling fluid types are used, including water-based and oil-based drilling muds (WBDMs and OBDMs).[6] With increasingly stringent environmental regulations, environmentally friendly and high-performance WBDMs are essential. Basic WBDM systems contain water as a base fluid, clays, and other chemicals.[7,8] Although WBDMs are preferred over OBDMs, however, there are several challenges such as drilling the shale layers which can conceivably cause wellbore instability due to clay−water interaction.[9,10]

During drilling, one of the severe problems is the increase in drilling mud invasion into the formation and inadequate control of fluid filtration properties. During filtration, solid particles in the drilling mud settle on the borehole wall and form a thin mud cake. The mud cake is the first barrier to prevent the increase of drilling mud filtration due to its low permeability.[11−14] Increasing drilling mud filtrates generally causes various problems such as damage to the oil production zones, fluid invasion into water-sensitive layers such as shales, and causing the drill string to be stuck due to thick mud cake formation.[15,16] Due to the importance of the topic, researchers have concentrated on nanoparticles (NPs) as a new additive to reduce fluid loss.[17−23]

Moreover, the nanomaterial in drilling fluids has no destructive impact on the risk of contamination of underground

Received: September 2, 2022
Accepted: November 8, 2022
Published: November 17, 2022

https://doi.org/10.1021/acsomega.2c05688
ACS Omega 2022, 7, 44223−44240

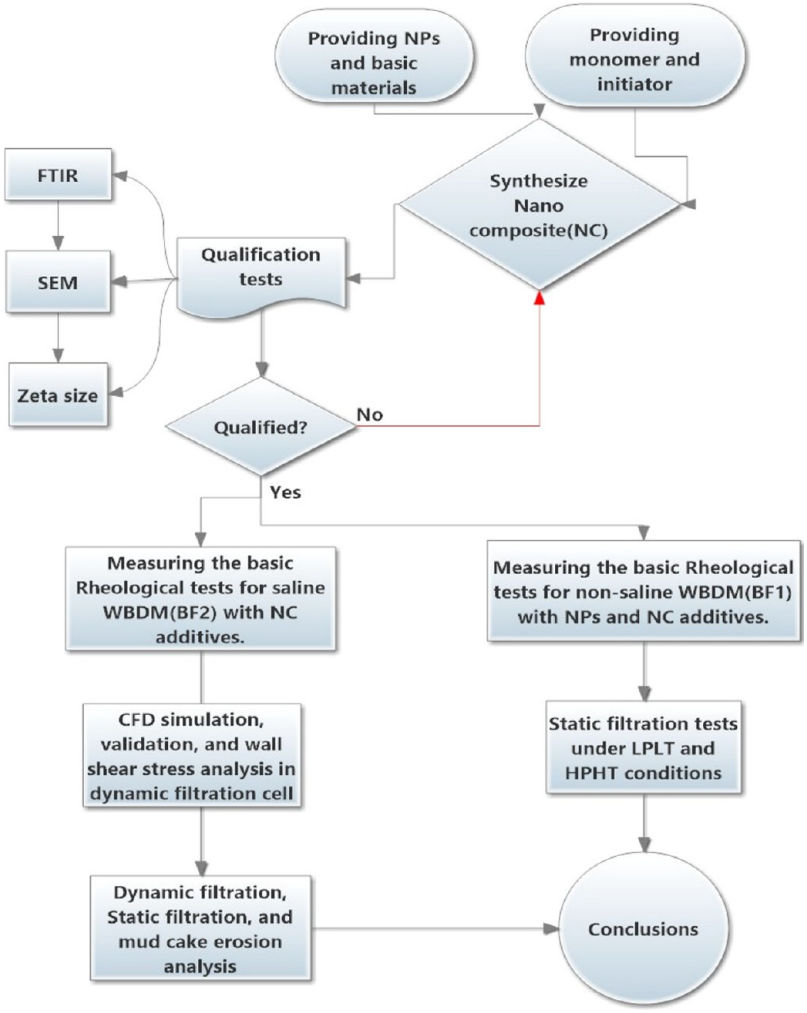

Figure 1. Schematic diagram of preparation and characterization of the NC and different stages of work until the final results.

freshwater during drilling. The reason for using NPs to reduce filtration and fluid loss is to reduce the deposited mud cake permeability on the wellbore by improving rheological properties and the pore blocking mechanism.[24−26] Alvi et al. investigated the effect of iron oxide NPs on the characteristics of OBDMs.[27] Bayat et al. evaluated the rheological and filtration properties of polymeric WBDMs treated by various NPs.[28] Moreover, the nanosilica is widely used as a low-cost additive in drilling fluid to overcome clay swelling and formation damage.[29] Correspondingly, rheological control is essential for the proper transfer of drilling cuttings and the hole-cleaning process. Adequate frictional drag force to carry cuttings has a vital role of drilling fluid provided by drilling mud viscosifiers. Therefore, introducing any new additive to control a fluid property should also improve other drilling mud roles.[30,31]

Polymers have also been used in several studies to improve the rheological behavior of WBDMs.[32−36] Some polymers like polyanionic cellulose, xanthan gum, carboxymethyl cellulose (CMC), and latexes have been widely used to improve the drilling fluid's rheological and filtration characteristics. The novel advanced methodologies to study the rheological behavior of complex fluids can be found in recent studies.[2,37] Lie et al. investigated the effect of carboxymethyl chitosan as an eco-friendly biopolymer to control the rheological and filtration properties of bentonite water-based drilling fluids.[29] However, polymer alone may not control drilling mud properties under down-hole conditions due to high temperatures at the bottom of the well. Furthermore, polymers may cause an excessive increase in the drilling mud's viscosity, increasing the fluid flow pressure drop. On the other hand, most of the prominent polymers used in the drilling industry may show less efficiency in high-salinity environments. Therefore, researchers have focused on synthesizing nanocomposites (NCs) such as acrylamide-based NCs to improve the filtration properties of drilling fluids.[38−41] Hamed Movahedi et al. evaluated the filtration control of WBDFs using a graphene-based nanocomposite under static and dynamic conditions.[38] The obtained results showed that the addition of the 0.7 wt % GO-PAM NC could reduce the erosion rate of the mud cake by more than 60% under turbulent flow conditions, while this value was 20% for GO nanosheets in the same concentration. Mao et al. have synthesized an acrylamide polymer-based silica NC, which has appropriate filtration and rheological properties.[42] An et al. grafted an acrylamide polymer on the surface of nanosilica to increase the durability of the polymer in the saline medium.[43] Fahime Kamali et al. investigated the efficiency of the Fe_3O_4-CMC NC on the rheological and filtration properties of water-based drilling fluids.[44] Fe_3O_4-CMC was synthesized by the coprecipitation method in their study. They showed that the synthesized NC can considerably improve the viscosity, filtration volume, and cake thickness.

https://doi.org/10.1021/acsomega.2c05688
ACS Omega 2022, 7, 44223−44240

This study evaluates a polyacrylamide-silica (PAM-S) NC as a new additive to control the filtration properties of bentonite-WBDM under different salinity conditions. Mesoporous nanosilica was chosen to be used as a NP in the structure of the NC. The low cost of nanosilica and its low environmental effects instead of polymer alone make the proposed method more efficient. Therefore, the novelty of the current work is proof of PAM-S efficiency through various tests under normal and high-pressure high-temperature (HPHT) conditions. Moreover, as can be seen in the literature, studies generally have focused on API static filtration for proving the NP/polymer additives used. However, one of the main essential properties of drilling fluids that should be studied is the filter cake characteristics such as tightness and erodibility under different laminar or turbulent shear forces. For instance, increasing the filtrate flux may create a consolidated or tight filter cake with sufficient resistance against erosion.[45] However, decreasing filter cake permeability using NPs reduces the filtrate flux, forming a mud cake with less consolidation, which is more erodible against the shear flow. Therefore, it is crucial to evaluate the cake erodibility for any new additive.

2. MATERIALS AND METHODS

2.1. Materials. Sodium montmorillonite clay is a natural smectic aluminosilicate used as the most popular additive in WBDMs to give better rheological properties. Simple drilling mud is generally made of water and bentonite at a specified ratio.

Investigation of the effect of different additives such as nanomaterials on WBDM, bentonite's structure, and basic chemistry must first be described. Bentonite is the trading name for sodium montmorillonite, the most popular clay mineral used in drilling fluids. The structure of clay minerals consists of layers formed by silica and alumina sheets.[46,47] Clay particles consist of a stack of parallel unit layers. The thickness of each layer is almost 10 angstroms (Å), and each stack consists of multiple layers. Each clay layer is very flexible and thin, which means that 1 g of clay has a large surface area. The surface charge in bentonite clay plays an essential role in hydration phenomena. Bentonite can be dispersed in water entirely when the salinity and ion concentrations such as Ca^{2+} and Na^{+} are well controlled. The flocculation or aggregation of bentonite plates may have occurred because of improper control of bentonite concentration or water salinity.[46]

Mesoporous silica with 20−30 nm was obtained from Sigma-Aldrich. The main reason for selecting this type of NP in this study is its abundance and lower cost compared to other similar NPs. Moreover, mesoporous NPs have a solid framework with a porous structure and a large surface area, allowing different functional groups' attachment. Other drilling fluid additives such as calcium chloride ($CaCl_2$) were also prepared.

2.2. Preparation of the PAM-S NC. For the preparation of the NC, the silica NPs were first functionalized. In the first step, 20 g of nanosilica with 900 mL of cyclohexane and 100 mL of water were mixed for 1 hour using the sonication method. In the second step, 25 mL of methacryloxypropyltrimethoxysilane was added to 100 mL of cyclohexane, and then it was added to the first solution. Finally, modified NPs were separated, washed with water and ethanol, and dried in an oven at 80 °C for 8 h. In the last step, 25 g of acrylamide, 0.02 g of methylene-bis-acrylamide, 0.01 g of ammonium persulfate, and 25 g of deionized water with 2.5 g of functionalized NPs were mixed and stirred for 20 min. Then, the obtained mixture was poured in a balloon equipped with a mixer. The mixture was heated up to 65 °C utilizing a water bath for 24 h. In the end, the prepared sample was washed with water and ethanol and then dried.[48,49] It should be noted that the given values are based on the trial-and-error method to obtain the best results. Figure 1 shows the design's schematic and how to achieve the final products and results of this work.

2.3. Formulation of the Drilling Fluid. As mentioned before, WBDMs contain water as a continuous phase and other additives for controlling properties like viscosity and filtration. Simple WBDM with freshwater and bentonite clay was prepared as a base drilling fluid for comparisons. To prepare a base fluid (BF1), 20 g of bentonite and 10 g of barite were added to 500 mL of distilled water and mixed thoroughly using a Hamilton beach mixer at a speed of 12,000 rpm. For the preparation of WBDM with nanoadditives, before adding solid powders to freshwater, silica NPs with specific concentrations were added to water and sonicated at room temperature to prepare a homogeneous suspension.[19] The nanofluid was then poured into the Hamilton beach mixer, and other additives at the same concentration in the base fluid were added to the mixture.

Salt contamination has become the most critical challenge faced by WBDMs under extreme salinity which can considerably reduce the rheological and filtration properties.[35,50,51] Hence, in this study, we analyzed the impact of $CaCl_2$ contamination on bentonite dispersion and filtration properties. Because the BF1sample showed an out-of-control fluid loss in media with higher salinity during base tests measurement, a second-base fluid (BF2) was prepared with a higher bentonite concentration (9 wt %). Due to the higher concentration of bentonite in BF1, the cake thickness measurement under dynamic filtration and shear flow conditions could be performed with minimum error.

Different types of WBDM formulations with their additives are shown in Table 1. Rheology and filtration characteristics of these fluids were investigated and compared in this study.

Table 1. WBDM Sample Formulations with Their Additives

mud sample	formulation
BF1	3.8 wt % bentonite +1.9 wt % barite+500 cc water
BF2	9 wt % bentonite+500 cc water
S1	BF1 + 0.038 wt % SiO_2
S2	BF1 + 0.075 wt % SiO_2
S3	BF1 + 0.15 wt % SiO_2
S4	BF1 + 0.28 wt % SiO_2
S5	BF1 + 1.9 wt % SiO_2
S6	BF1 + 0.038 wt % PAM-S
S7	BF1 + 0.15 wt % PAM-S
S8	BF1 + 0.28 wt % PAM-S

2.4. Analysis and Characterization. Fourier transform infrared spectrometry (FTIR) was implemented to prove polyacrylamide's presence on the surface of silica NPs. Dynamic light scattering (DLS) studies were also conducted for size distribution analysis of NPs. Scanning electron microscopy (SEM) was used to analyze the surface morphologies of nanomaterials and filter cakes in this study.

2.5. Zeta Potential and Swelling Test. The high salt contamination in drilling fluids affects bentonite hydration resulting in flocculation and low filtration properties. As the presence of counter ions (cation) in the solution increases, the electrical double layer around particles shrinks due to the neutralization of particle surface charge. Hence, the particle zeta potential decreases, reducing repulsive forces among particles. Consequently, the aggregation of clay sheets occurs in solution

https://doi.org/10.1021/acsomega.2c05688
ACS Omega 2022, 7, 44223−44240

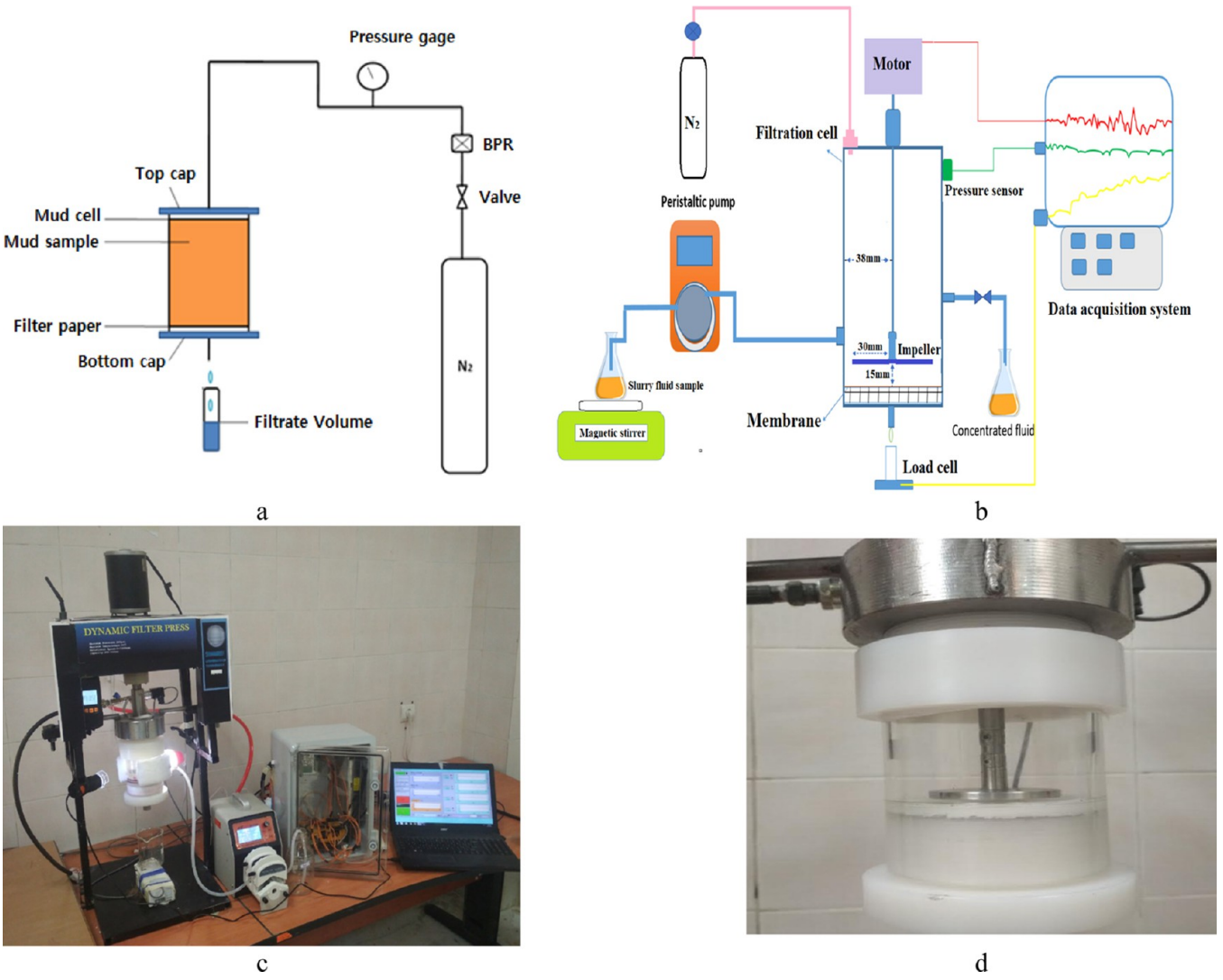

Figure 2. Schematic of the API Filter press (a), schematic of the dynamic filter press (b), static and dynamic filtration apparatus (c), and transparent filtration cell (d).

resulting in instability and poor filtration properties. Therefore, the zeta potential and clay swelling characteristics must be thoroughly analyzed.

2.6. Rheology and Filtration. The rheological measurements of mud samples under a low shear rate were performed using a Brookfield viscometer. The key rheological parameters such as yield point (YP) and apparent viscosity (AV) were obtained using an FANN viscometer (model 35). The filtration properties of WBDM samples were measured under both low-pressure/low-temperature (LPLT) and HPHT conditions. The filter press apparatus was utilized to measure filtration characteristics like fluid loss volume and thickness of the filter cake for the WBDM samples based on API standards. The filtration tests under LPLT conditions were performed at 100 psi and 25 °C. Static filtration testing is used as a standard method for assessing drilling mud filtration quality in actual conditions. It means that drilling mud with a high amount of measured filtration losses is not proper for actual operation. Figure 2a shows the schematic of the static filtration apparatus. The pressure source is supplied from a cylinder containing nitrogen gas. The required pressure is applied to the filtration cell by using a back pressure regulator. By applying pressure and starting the filtration test, the filtrate loss at the outlet of the cell is measured by a scaled cylinder. For HPHT conditions, the pressure and temperature were regulated at 3400 kPa and 90 °C, respectively.[11] Dynamic filtration has also been conducted to investigate the effect of shear flow on filtration parameters such as the flux rate and cake erosion. The dynamic system includes a filtration cell equipped with mixing equipment (see Figure 2b). The filtration is performed under constant pressure, and at the same time, as the disk rotates inside the filtration cell, a shear flow is applied on the surface of the filter paper. The distance between the disk and the filter paper is 15 mm, and the disk diameter and thickness are 60 and 5 mm, respectively. The electrical motor can adjust the rotating speed up to 2000 rpm. An increase in the solid content in the cell occurs during dynamic filtration due to cake erosion. Thus, a peristaltic pump was utilized to discharge the concentrated slurry out of the cell (see Figure 2c). During dynamic filtration, the turbulent flow created by the rotation can represent the shear flow inside the well. Therefore, dynamic filtration can provide a better insight into the effect of new additives on the drilling fluid in actual conditions. Dynamic filtration tests were also conducted under 680 kPa pressure and 25 °C temperature. Moreover, a transparent cell was used to better characterize the flow field inside the filtration cell (see Figure 2d).

https://doi.org/10.1021/acsomega.2c05688
ACS Omega 2022, 7, 44223−44240

2.7. Model and Simulation. During static filtration, the cumulative fluid loss rate is proportional to square roots of time and is described by the following equation:[46]

$$V_f = A\sqrt{\frac{2kt(F_{SolidCake} - F_{SolidMud})\Delta P_f}{\mu F_{SolidMud}}} \quad (1)$$

where t is the interval time, k is the permeability of the mud cake, ΔP_f is differential pressure, μ is the viscosity of the mud filtrate, A is the cross-sectional area, and $F_{SolidCake}$ and $F_{SolidMud}$ are the volume fraction of solids in the mud cake and drilling fluid, respectively.

Each particle is subjected to two main forces during dynamic filtration: the tangential shear forces (F_x) generated by disk rotation and vertical drag force (F_y) due to the filtrate flux passed through the membrane. The shear forces applied to particles attached to the cake can be modeled by wall shear stress (WSS). Moreover, Stokes's law can also describe the drag forces due to the filtrate flux as follows:

$$F_y = \alpha\pi d_p^2 \times \frac{1}{8}\rho_p V_p^2 \times \frac{24}{Re_p} \quad (2)$$

where α is a shape factor for considering the nonspherical particles, d_p, ρ_p, and Re_p are the particle diameter, density, and Reynolds number, respectively, and V_p is the filtrate flux.

The tangential force due to the shear flow can be expressed as:

$$F_x = \alpha\pi d_p^2 \tau_w \quad (3)$$

where τ_w is the WSS.

If the forces exerted to particles by filtrate flux exceed the shear force, the cake will continue to grow under the following conditions:

$$F_x \ll fF_y \quad (4)$$

where f is the friction coefficient between particles.

Under equilibrium conditions, the cake growth does not continue. The equilibrium cake thickness (CTe) can be calculated as:

$$F_x = F_y \rightarrow \tau_w = \frac{3\mu}{d_p}V_p \quad (5)$$

Based on Darcy's law, the filtrate flux is inversely proportional to the cake thickness, thus:

$$CT_e = \beta\frac{1}{\tau_w} \quad (6)$$

where β can be obtained by experimental data.

To calculate the WSS exerted on the membrane surface, the computational fluid dynamic (CFD) technique was implemented to solve the flow field inside the filtration cell and obtain the required parameters. CFD simulation needs to be validated to be considered a reliable method. By considering fluid rheology, the fluid flow inside the filtration cell can be modeled as single-phase flow.

The three-dimensional geometry of the filtration cell with a rotating disk was discretized by approximately 0.5 million structured mesh (Figure 3). The ANSYS FLUENT package was used to simulate the flow field by implementing the segregated, transient-state, and implicit numerical solver. Moreover, the governing equations, including continuity and momentum, were coupled using the SIMPLE algorithm. Because swirling and eddy flow created by the rotating disk significantly affect the WSS distribution, the large eddy simulation was employed as the turbulent model to capture the eddy flows accurately.[45] No-slip stationary wall boundary was applied to all boundaries while the moving wall conditions were assigned to rotating disk faces. The convergence criteria were that the residuals of parameters were below 1.0 × 10−5.

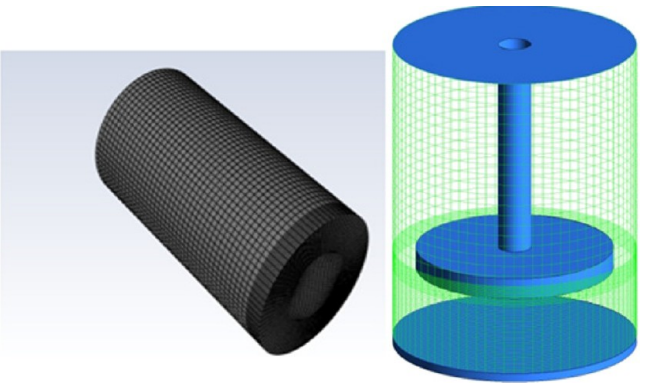

Figure 3. Geometry of the filtration cell with structured meshes.

3. RESULTS AND DISCUSSION

3.1. Characterization. Figure 4 shows the results of FTIR analysis for silica NPs, PAM, and PAM-S. As shown in Figure 4a, the peak at 3450 cm^{-1} is related to the hydroxyl groups (Si−OH) and another peak at 1072 cm^{-1} indicates the presence of Si−O−Si combinations. The peaks at 3453, 2927, and 1657 cm^{-1} are related to N−H bending, $-CH_2$ stretching, and N−H bending in $-CONH_2$ of the PAM hydrogel, respectively (Figure 4b). In the NC, the peak in the range of 3420 cm^{-1} indicates the oscillation of OH groups and NH groups of amides. Other peaks at 1710 cm^{-1} and 1460 cm^{-1} are related to amide carbonyl groups (Figure 4c).[52,53]

The surface morphology of silica NPs and the synthesized NC is shown in Figure 5a,b. The rough surface of the NC indicates that the composite is covered by NPs. PAM-S has a wide particle size distribution. The average sizes of NPs and NC were obtained as 20 nm and 140.5 nm, respectively (Figure 5c). As can be seen, the polymer coating is well placed on the silica NPs so that the mean particle diameter shows a significant increase.

3.2. Zeta Potential and Clay Swelling. Figure 6a shows the variation of the zeta potential of the BF2 with different $CaCl_2$ concentrations. The salinity ratio (SR) is defined as the salt to clay ratio in the solution.[45] As can be seen, for $CaCl_2$ concentration above SR = 0.2, the presence of counterions in the solution is sufficient to neutralize clay surface charge. The clay swelling phenomenon occurs by forming molecular water layers on the surface of clay minerals and depends on the type and concentration of cations in the solution. To investigate the effect of salt on swelling phenomena, bentonite was mixed with a series of solutions containing $CaCl_2$. After 1 day, the height of deposited clay in each sample represents the status of clay swelling. Figure 6b shows the variation in the magnitude of clay swelling with salt concentration. As is shown, the increasing salt concentration corresponds to a decrease in the magnitude of clay swelling. Moreover, the effect of silica NP concentration on clay swelling was also investigated. A series of solutions containing 0.1 gr bentonite and different contents of NPs were prepared. As shown in Figure 6c, NPs prevent further swelling of the clay particles. Generally, the distance between the clay plates is less than 2 nm after complete swelling.[54] Hence, as

https://doi.org/10.1021/acsomega.2c05688
ACS Omega 2022, 7, 44223−44240

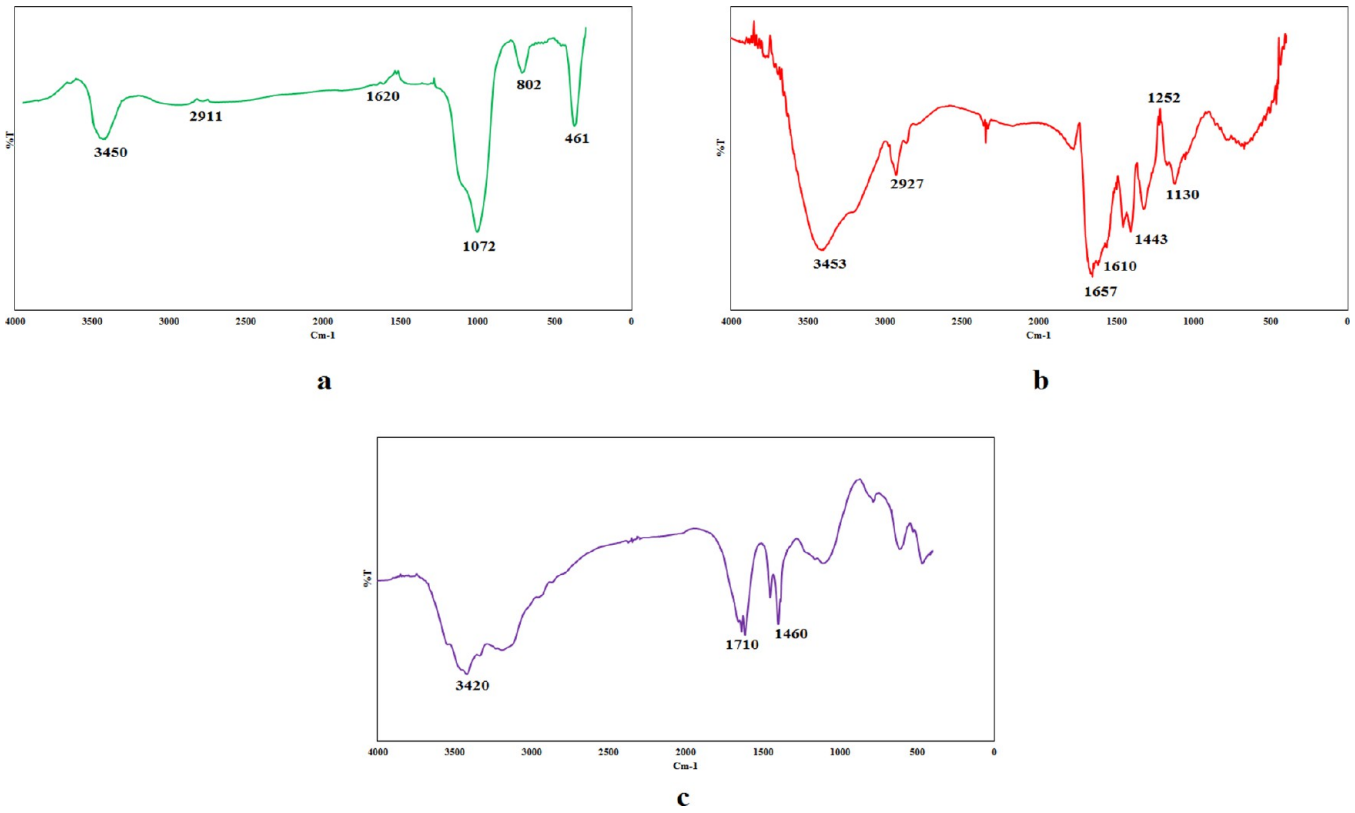

Figure 4. FTIR spectra of silica NPs (a), PAM (b(, and PAM-S (c).

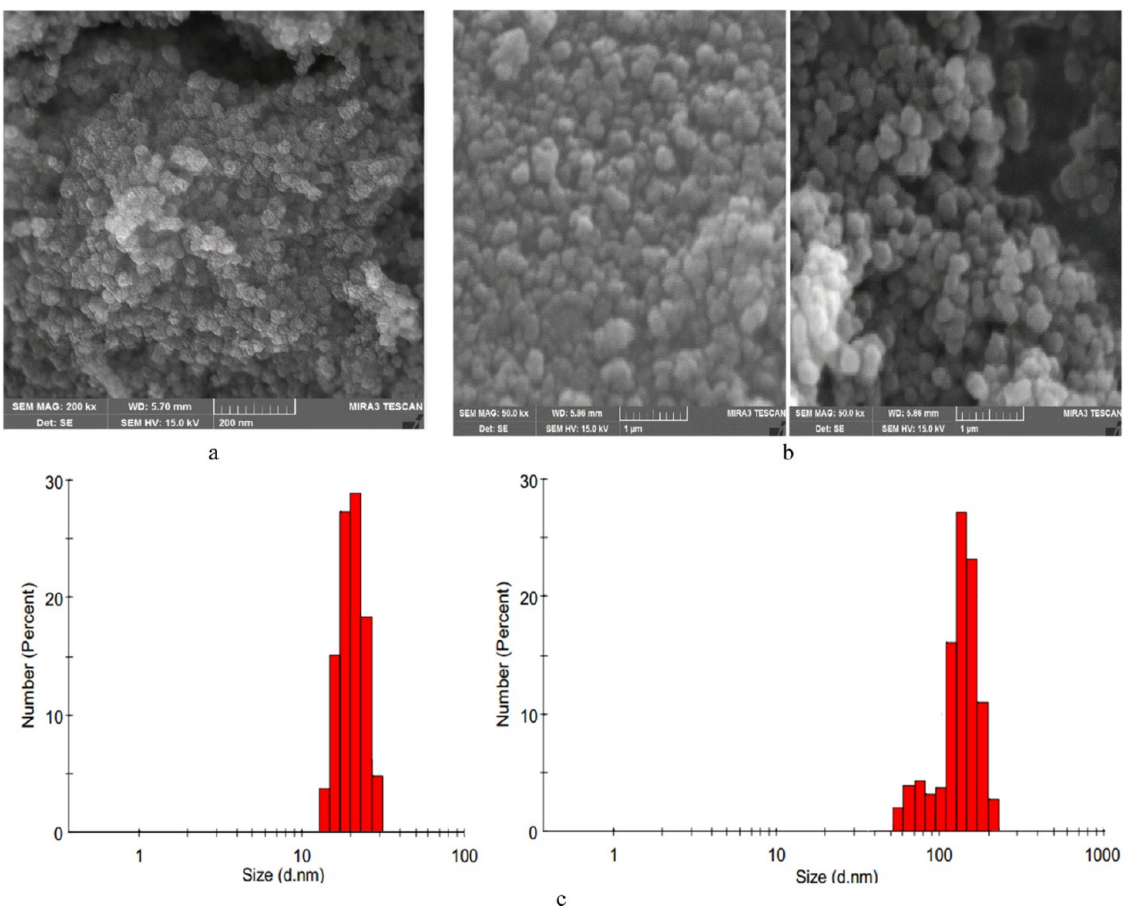

Figure 5. SEM image of silica NPs (a), SEM image of PAM-S (b), and particle size distribution of silica NPs (c-left) and NC (c-right).

https://doi.org/10.1021/acsomega.2c05688
ACS Omega 2022, 7, 44223−44240

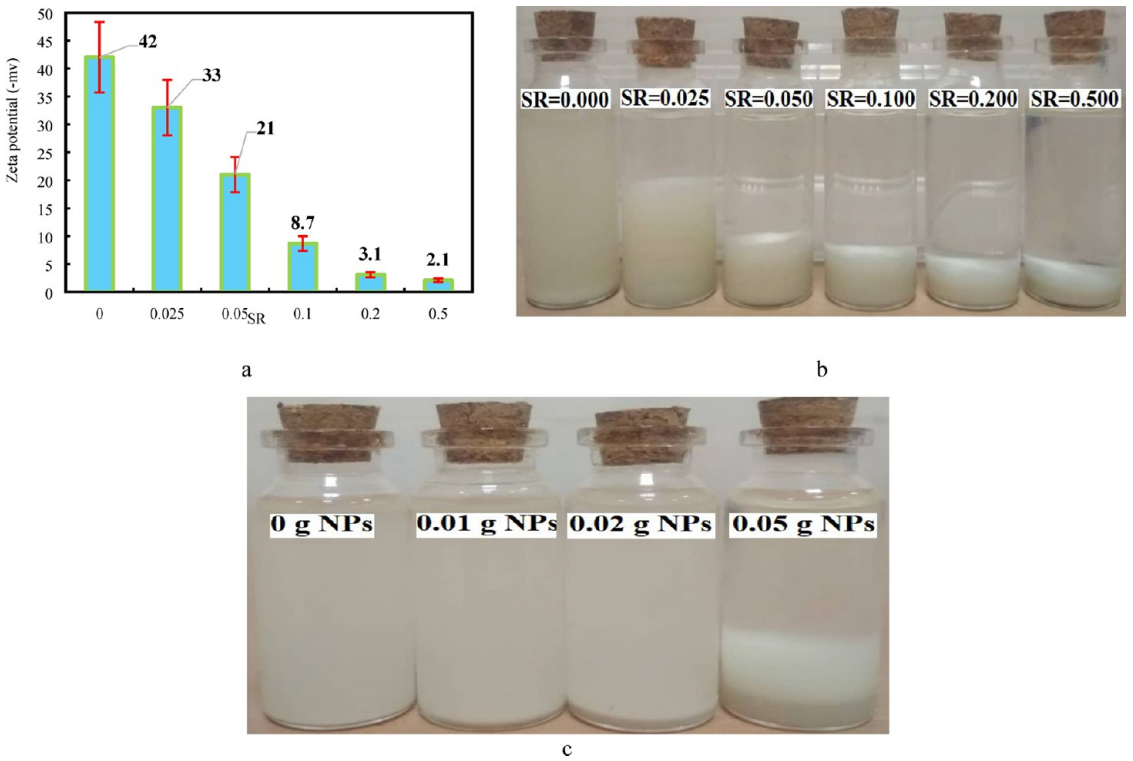

Figure 6. Variation of zeta potential (a) and variation of clay swelling with salt concentration (b) and silica NPs (c).

Table 2. Rheological Data of Drilling Fluid Samples

RPM	BF1	S1	S2	S3	S4	S5	S6	S7	S8
	viscosity (cp)								
2	220	131.1	124.8	72.3	84.3	110	296	488	611
3	139	116.2	95.8	49.5	63.2	79.8	255	390	491
4	112.7	95.1	77.1	37.5	54.2	71.5	204	304	446
5	81.2	78.6	63.8	27	43.5	60.4	181	236	338.4
6	61.2	56.3	44.4	21.7	32.6	48.6	146	194	290
10	53	46	36.2	15.7	28.2	51	116	132	256.5
12	46.2	38.9	32.4	13.25	21.1	39.4	91	112	217.4
20	37.2	25.6	24.6	10.2	17.2	29.6	64.3	83	159.2
30	27.2	19.5	18.4	8.86	12.3	25.3	48.2	64	115.2
50	19.4	12.62	11.8	7.24	10.8	20.6	26.25	51	83.5
60	12.5	6.2	5.6	6.57	9.88	17.1	19.2	28.2	58.2
100	7.26	--	--	5.89	8.91	14.8	12.4	14.1	28.5

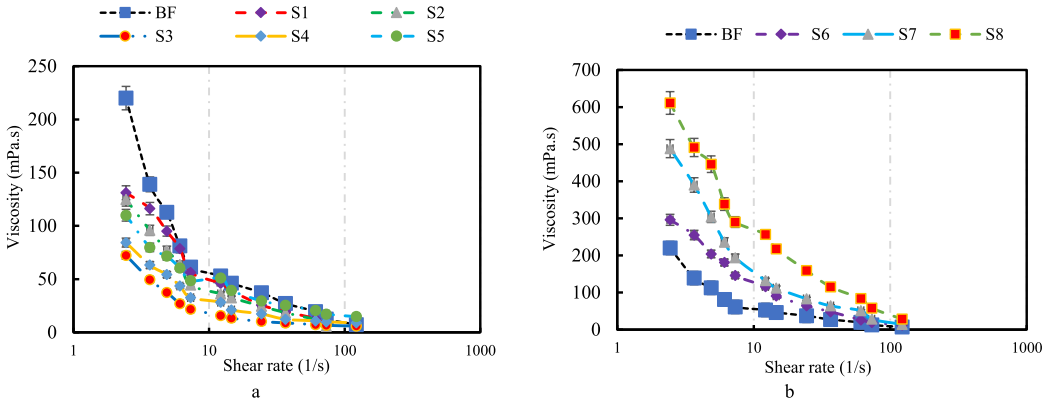

Figure 7. Variation of viscosity with applied shear rate for different concentrations of nanosilica (a) and different fluid samples prepared with PAM-S (b).

https://doi.org/10.1021/acsomega.2c05688
ACS Omega 2022, 7, 44223−44240

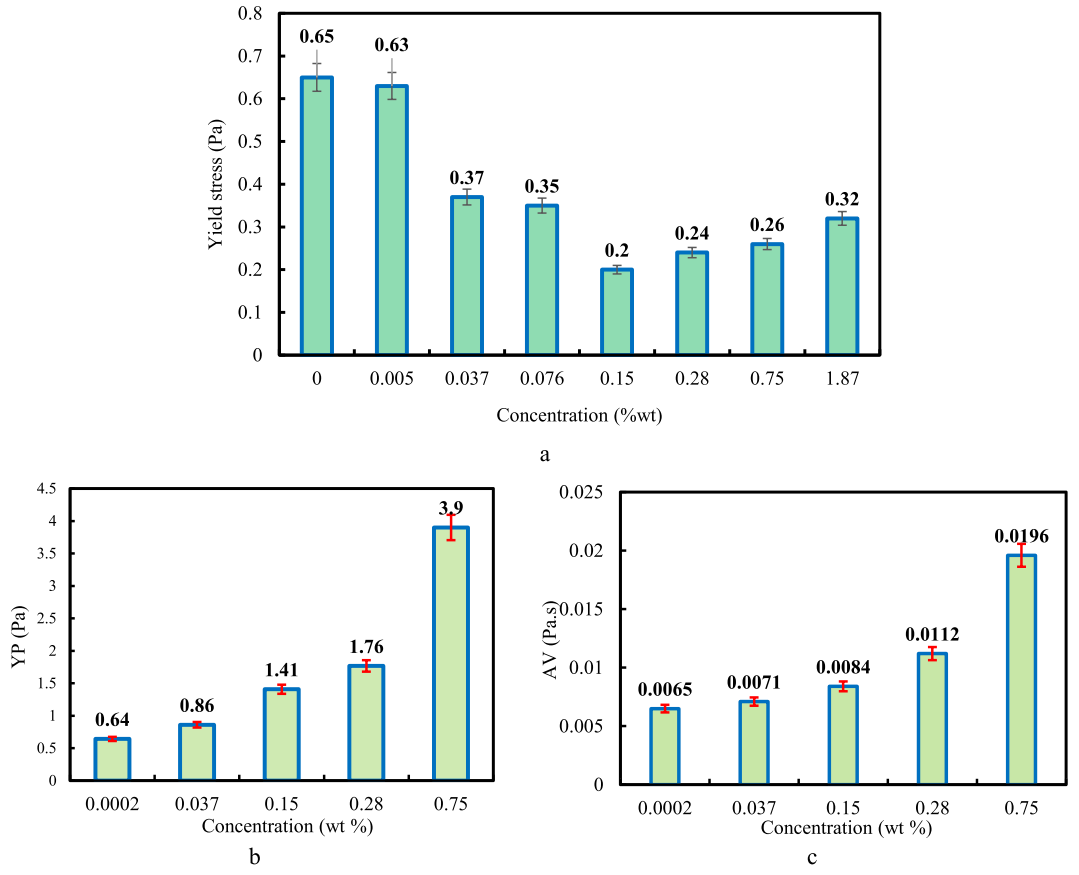

Figure 8. Effect of silica NP concentration on drilling fluid YP (a) and PAM-S concentration on YP (b) and AV (c) of the base fluid.

the size of NPs is more than the distance between clay sheets, it can affect the swelling phenomena.

3.3. Rheological and Filtration of Nonsaline WBDM.

3.3.1. Rheological Properties. Rheological data obtained from the Brookfield rheometer are summarized in Table 2. The variations of drilling fluid samples' viscosity at different shear rates are shown in Figure 7a. It is clear that viscosity is not constant at various shear rates, which indicates that the drilling fluids have non-Newtonian rheological behavior. It can be seen that as the shear rate increases, the viscosity is decreased, and thus all fluid samples have shear thinning behavior. The results also show that the presence of silica NPs at concentration below 2 g (i.e., S1−S4 samples) has unfavorable impact on rheological properties of WBDM. As discussed, due to the presence of NPs the hydration of clay particles does not proceed well. However, by adding NPs with a concentration higher than 10 g or 1.9 wt % (i.e., S5 sample), the drilling fluid viscosity increases because of the presence of more solid particles and mechanical friction between them. Figure 7b shows the effect of the NC on the viscosity of the drilling fluid. As shown, unlike silica NPs, PAM-S increases the viscosity of the drilling fluid at any concentration. Because of the presence of PAM in the NC structure, the fluid viscosity increases. Improving the drilling fluid viscosity near four times compared to the base fluid by adding just 4 g NC (0.75 wt %) confirms the effectiveness of PAM-S as a new additive. Moreover, the polymer on the surface of NPs causes the clay plates to tend to more aggregation, which increases the YP.

Figure 8a presents the effect of silica NPs on YP of WBDM. As is shown, NPs in drilling mud at a low concentration result in the reduction of YP. At high concentrations, the YP increases due to the presence of more solid particles in drilling mud. Figure 8b,c shows the variation of YP and AV with increasing the NC concentration. As is shown, at the concentration below 1 wt %, the YP and AV of the base fluid could improve by eight and four times, respectively.

Figure 9 shows the variation of AV and YP of the BF2 sample at different $CaCl_2$ concentrations. As is shown, the critical salt concentration for the base fluid is 0.7 wt %, in which the AV and YP reach the minimum value.

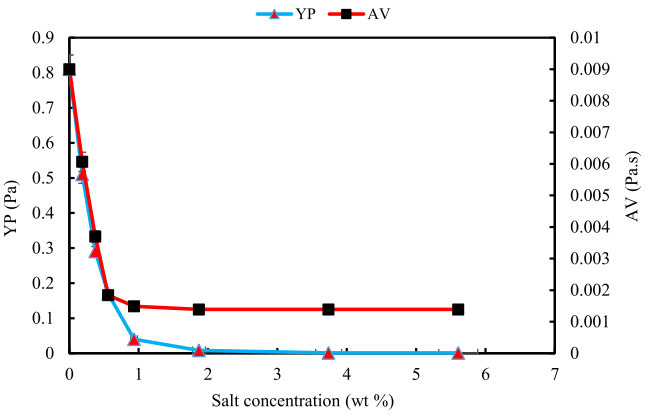

Figure 9. Variation of rheological properties of the base fluid with different salt concentrations.

3.3.2. Static Filtration Test Results. Figure 10a shows the variation of filtrate loss versus $t^{1/2}$ for different fluid samples prepared by silica NPs. It is shown that as nanosilica

https://doi.org/10.1021/acsomega.2c05688
ACS Omega 2022, 7, 44223−44240

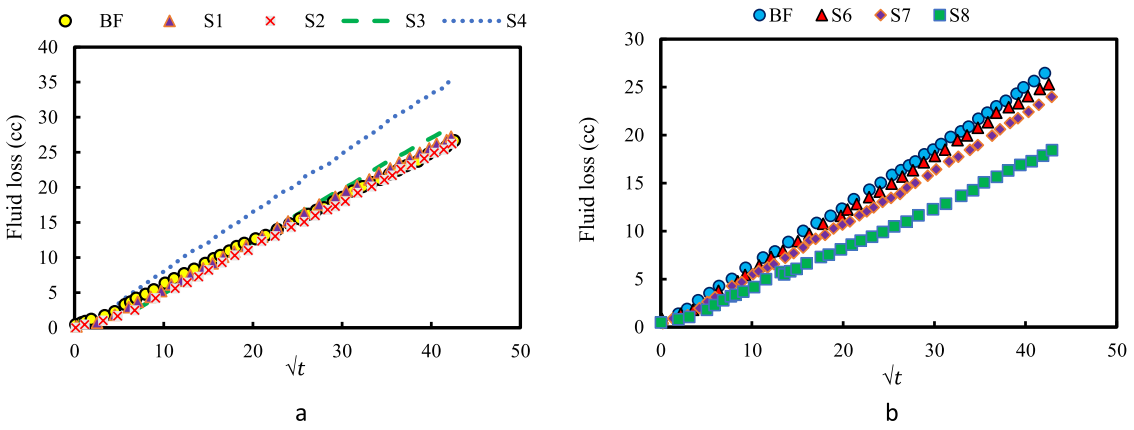

Figure 10. Variation in the rate of filtrate loss for different silica NPs-WBDM samples (a) and different fluid samples prepared by the NC (b).

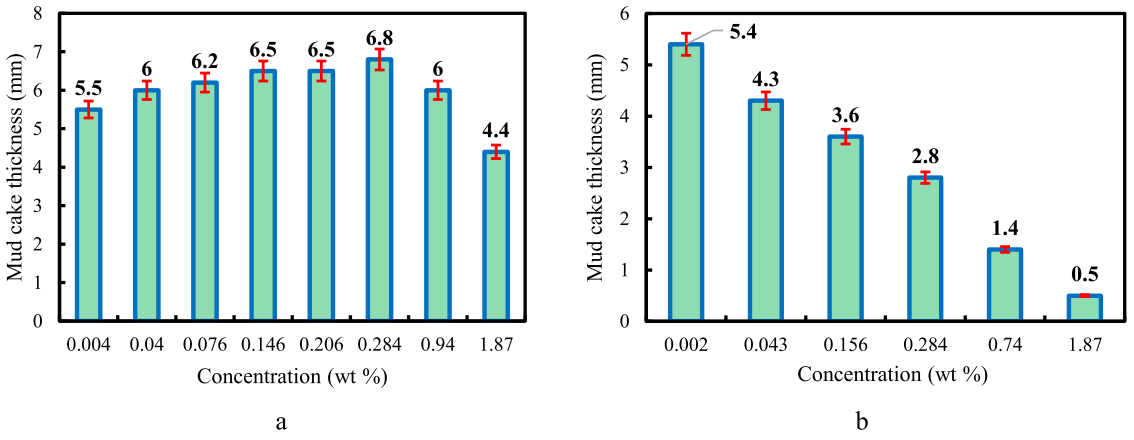

Figure 11. Effect of NP concentration on the thickness of the mud cake for silica NPs (a) and NC (b).

concentration increases, the rate of fluid loss increases so that the most amount of filtrate loss was observed for the S4 fluid sample. Dispersion of bentonite sheets in the drilling fluid induced by nanosilica leads to the increase of the fluid loss property. The effect of NC concentration on fluid loss is shown in Figure 10b. By increasing the NC concentration, the rate of fluid loss was decreased through either pore-blocking by NPs or increasing fluid viscosity and YP. One of the most critical parameters in controlling the drilling fluid filtration is reduction of the mud cake permeability. Reduction near 30% of fluid loss by adding just 1.5 g NC confirms that it has both economic and technical capabilities as a fluid loss control agent.

One of the important properties of drilling fluids is the thickness of the mud cake. Figure 11 indicates the effect of nanoadditives on the thickness of the drilling mud cake. As is shown, unlike silica NPs, PAM-S reduces the mud cake thickness at any concentration. The reduction of mud cake permeability as a result of adding NCs to drilling fluid leads to the reduction of the filtration rate. As a result, the fluid sample with a lower filtration rate has a lower filter cake thickness which can be considered as a significant advantage for this mud sample. Moreover, the lower permeate force due to low mud cake permeability makes the mud cake more erodible. It should be mentioned that the mud cake with a higher thickness can cause stuck pipe problems during drilling operations. Formation of a low-thickness mud cake on the wellbore wall with low permeability is more noticeable for environmental and industrial aspects.

The rate of filtrate loss decreased with time by the growth of the filter cake during the filtration process. To analyze the permeability of the mud cake, the flux variation passed through the mud cake has been studied. Figure 12 shows the variation of filtrate flux along with their fitted model for mud samples containing NCs. As shown, the flux rate decreases as NC concentration increases in mud samples. Meanwhile (as shown in Figure 11b), the thickness of the mud cake decreases as the NC concentration increases. Therefore, the developed NC could reduce the flux rate by reducing mud cake permeability as well as rheological improvement.

HPHT filtration tests were also performed in order to assess the applicability of nanoadditives under real conditions. Figure 13a shows the total filtrate loss of the drilling fluid containing silica NPs at different concentrations after 30 min under both LPLT and HPHT conditions. It can be observed that under HPHT conditions, the filtrate loss is much more significant because of the reduction of drilling fluid viscosity. Similar to LPLT conditions, the filtrate loss was increased by increasing the concentration of silica NPs. The total filtrate loss of drilling fluid containing different concentrations of NC after 30 min under both LPLT and HPHT conditions is demonstrated in Figure 13b. The reduction of filtrate loss under HPHT conditions at a low concentration well proves the performance of the NC at higher temperatures. As can be seen, the addition of 4 g NC (0.75 wt %) could reduce the total fluid loss from 26 to 7.4 cc under LPLT conditions and also could reduce it from 101 to 33 cc under HPHT conditions.

https://doi.org/10.1021/acsomega.2c05688
ACS Omega 2022, 7, 44223−44240

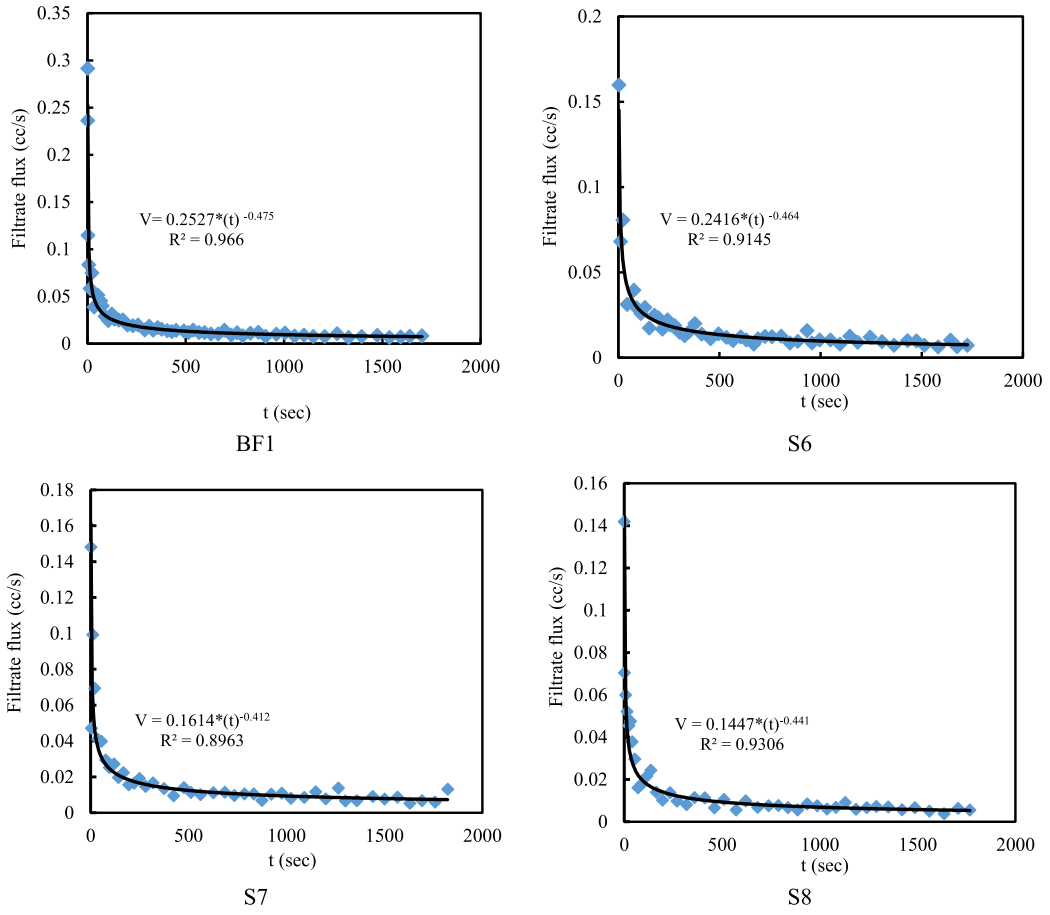

Figure 12. Variation of filtrate flux (bullet point) and corresponding model fitted (black line) for mud samples with the NC at low concentration.

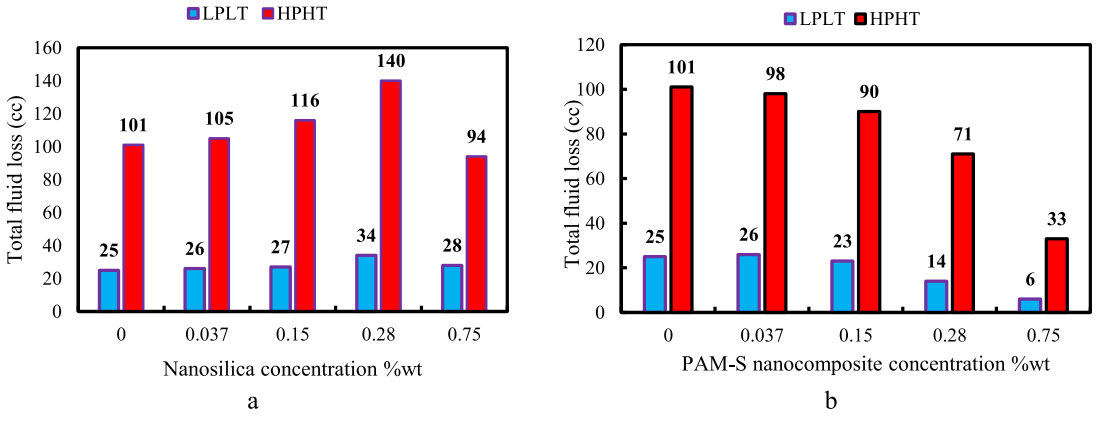

Figure 13. Total filtrate loss of the drilling fluid containing silica NPs under LPLT and HPHT conditions (a), and total filtrate loss of the drilling fluid containing NC under LPLT and HPHT conditions (b).

The surface SEM images of mud cakes are shown in Figure 14. As can be seen, the morphology of the surface of the base mud cake has open and heterogeneous cavities. For the mud sample prepared with an NC at low concentration (i.e., fluid sample S6), the cavities were not blocked well. However, for the mud sample prepared by an NC at a concentration of 1.5 g (i.e., fluid sample S8), the surface of the mud cake is smooth, and the main cavities are closed, which reduces the permeability of the filter cake and does not allow the fluid to penetrate the formation.

3.4. Effect of Salt Concentration. The performance of the PAM-S has been analyzed under different $CaCl_2$ concentrations. The variation of total filtrate loss and AV for the BF2 sample treated by 0.75, 1, and 1.5 wt % PAM-S at the different concentrations of $CaCl_2$ is shown in Figure 15a,b. As is shown, due to the reduction of bentonite properties in the salt concentration critical point, the total fluid loss was sharply increased for the base fluid at the 1 wt % of salt concentration. However, the NC could reduce the fluid loss by 60% at the 1.5 wt % concentration. The adsorption groups on the PAM-S could form hydrogen bonds with oxygen atoms on the surface of bentonite, and PAM could be firmly adsorbed on the surface of clay particles.[38] Therefore, the cation exchange capacity of bentonite clay is reduced and prevents the failure of filtration

https://doi.org/10.1021/acsomega.2c05688
ACS Omega 2022, 7, 44223−44240

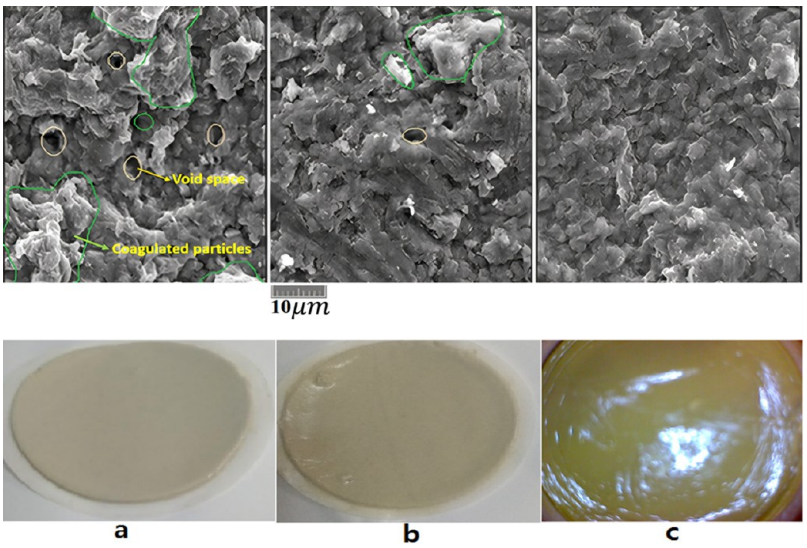

Figure 14. Surface SEM images of mud cakes, (a) base fluid, (b) WBDM containing 0.2 g NC (S6), and (c) WBDM containing 1.5 g NC (S8).

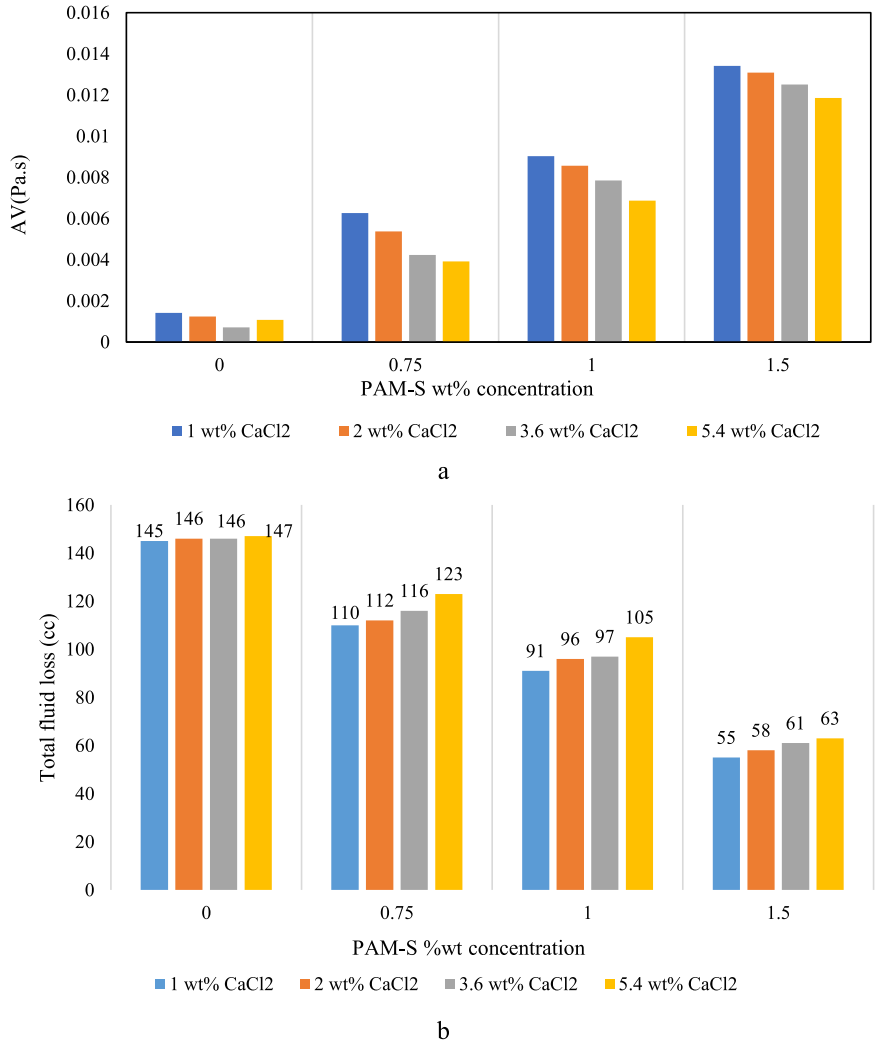

Figure 15. Effect of $CaCl_2$ concentration on AV (a) and total fluid loss (b) of BF2 treated by NC.

performance under Ca^{2+} contamination. Hence, the rheological and filtration properties are improved.

3.5. Dynamic Filtration. During the filtration process, because the velocity gradient applied to the fluid depends on the radius of the rotating disk and is minimal in the center, the cake thickness has a variable surface profile with the radius. Therefore, the WSS profiles should be determined using CFD simulation for each rotational speed. Hence, to obtain accurate

https://doi.org/10.1021/acsomega.2c05688
ACS Omega 2022, 7, 44223−44240

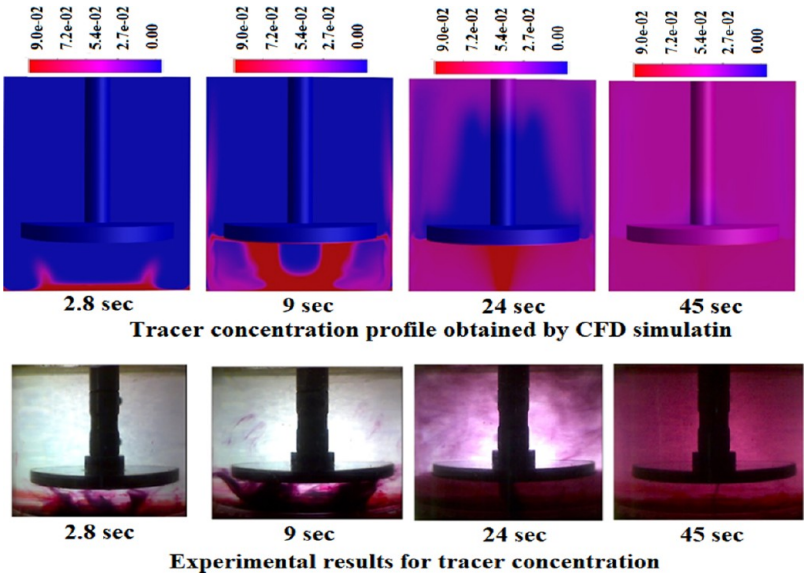

Figure 16. CFD simulation and experimental results for the mixing process at a rotating speed of 100 rpm.

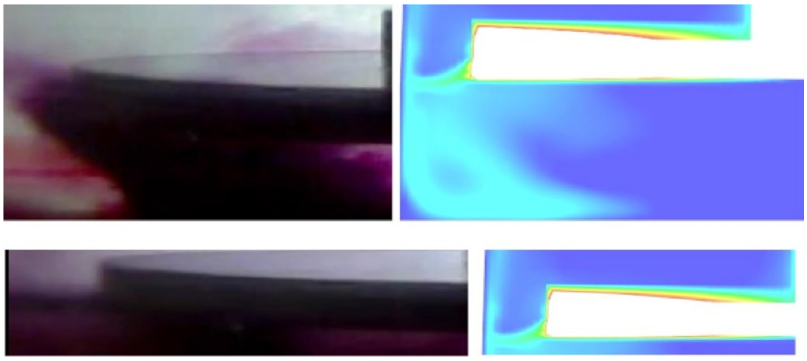

Figure 17. CFD simulation and experimental results of distribution of velocity at the edge of the rotating disk.

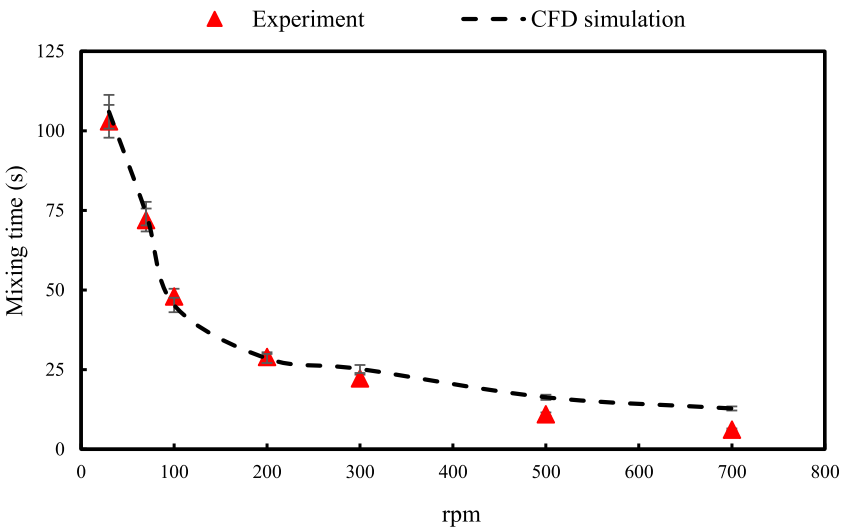

Figure 18. Comparison between CFD simulation and experimental results of the mixing time at different rotation speeds.

data from CFD, the numerical results need to be validated. For this purpose, the mixing time technique was used. It was implemented by injecting a tracer into the cell and measuring the required time for complete mixing at any disk rotation speed. Fluid mixing simulation was performed using the volume of fluid (VOF) model available in Fluent. This model was used to characterize the contact surface of two fluids.[55] A tracer (colored water) was injected through the end of the cell. To prevent instantaneous mixing and control the dispersion, the viscosity of the tracer was increased by adding a certain amount of

https://doi.org/10.1021/acsomega.2c05688
ACS Omega 2022, 7, 44223−44240

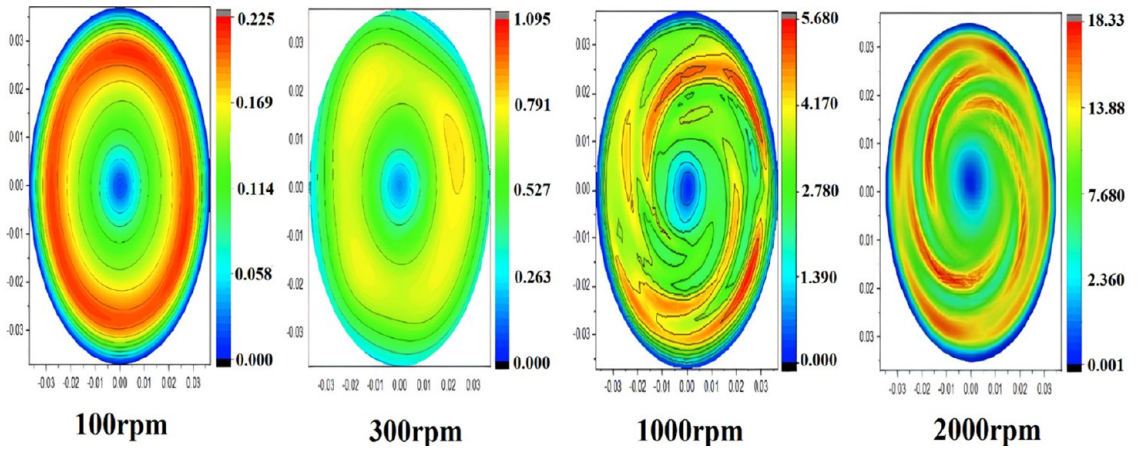

Figure 19. WSS distribution on the membrane surface at the different rotational speeds.

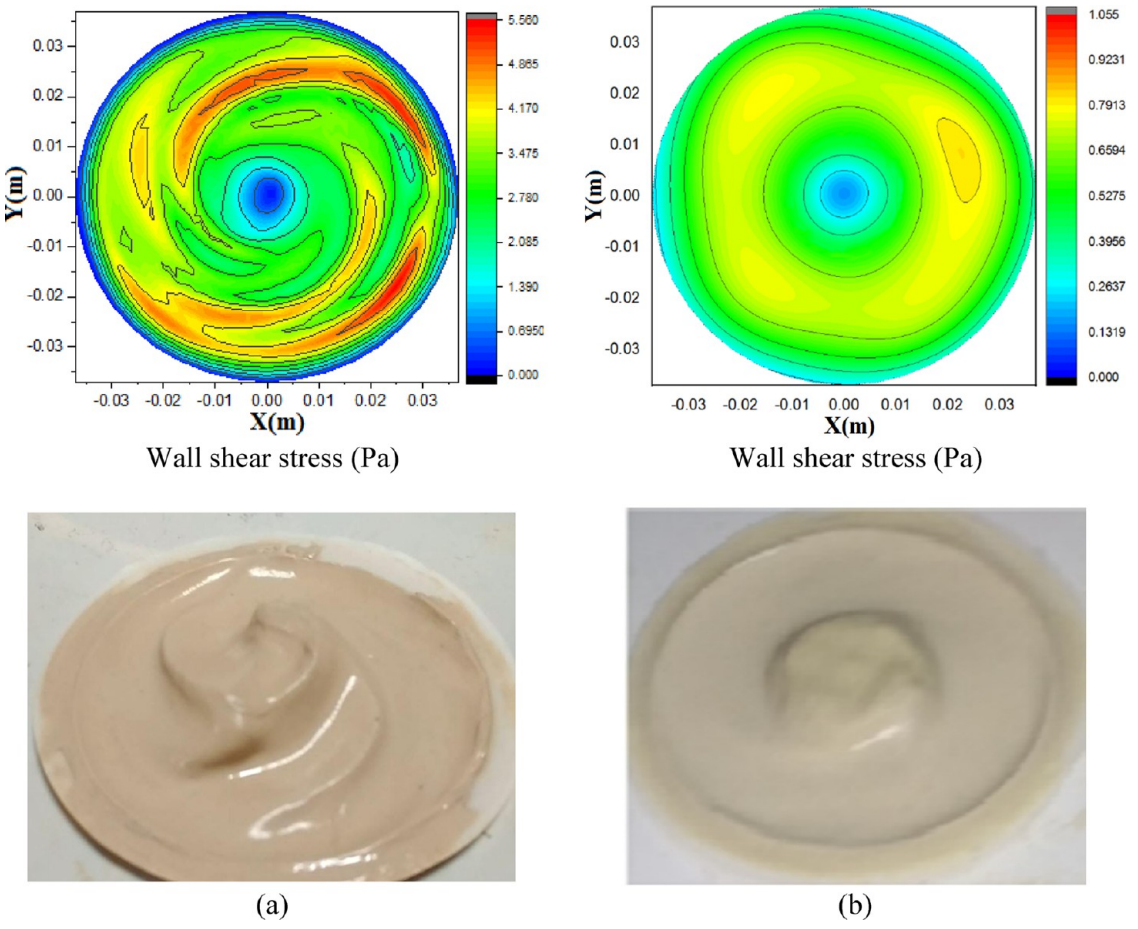

Figure 20. Wall shear stress (Pa) profile and surface pattern of the deposited cake at rotation speeds of (a) 1000 rpm (a) and 300 rpm (b).

polyacrylamide to three centipoises. Hence, the chief mechanism during the mixing process is advection induced by shear forces. Finally, by injecting a particular volume, the tracer film with a thickness of 2 mm was placed at the bottom of the cell. Because the filtration cell is transparent, the mixing of the two fluids is recorded by a camera until complete mixing occurs at each specified rotational speed. The mixing time in the simulation occurs when the same concentration distribution establishes throughout the cell. Finally, the calculated mixing time was compared with laboratory data. More details regarding the validation process of this system using the VOF model can be found elsewhere.[45] Figure 16 shows the comparison between experimental and simulation during the mixing process at 100 rpm. As revealed, the numerical simulation can accurately predict the trace of colored fluids.

Figure 17 also shows the trace of the colored fluid and calculated velocity by CFD at the edge of the rotating disk. As can be observed, at the time of capturing this shot, the shape of the flow field distribution completely matches with given numerical results. Hence, the numerical simulation could accurately present the flow field inside the filtration cell.

https://doi.org/10.1021/acsomega.2c05688
ACS Omega 2022, 7, 44223−44240

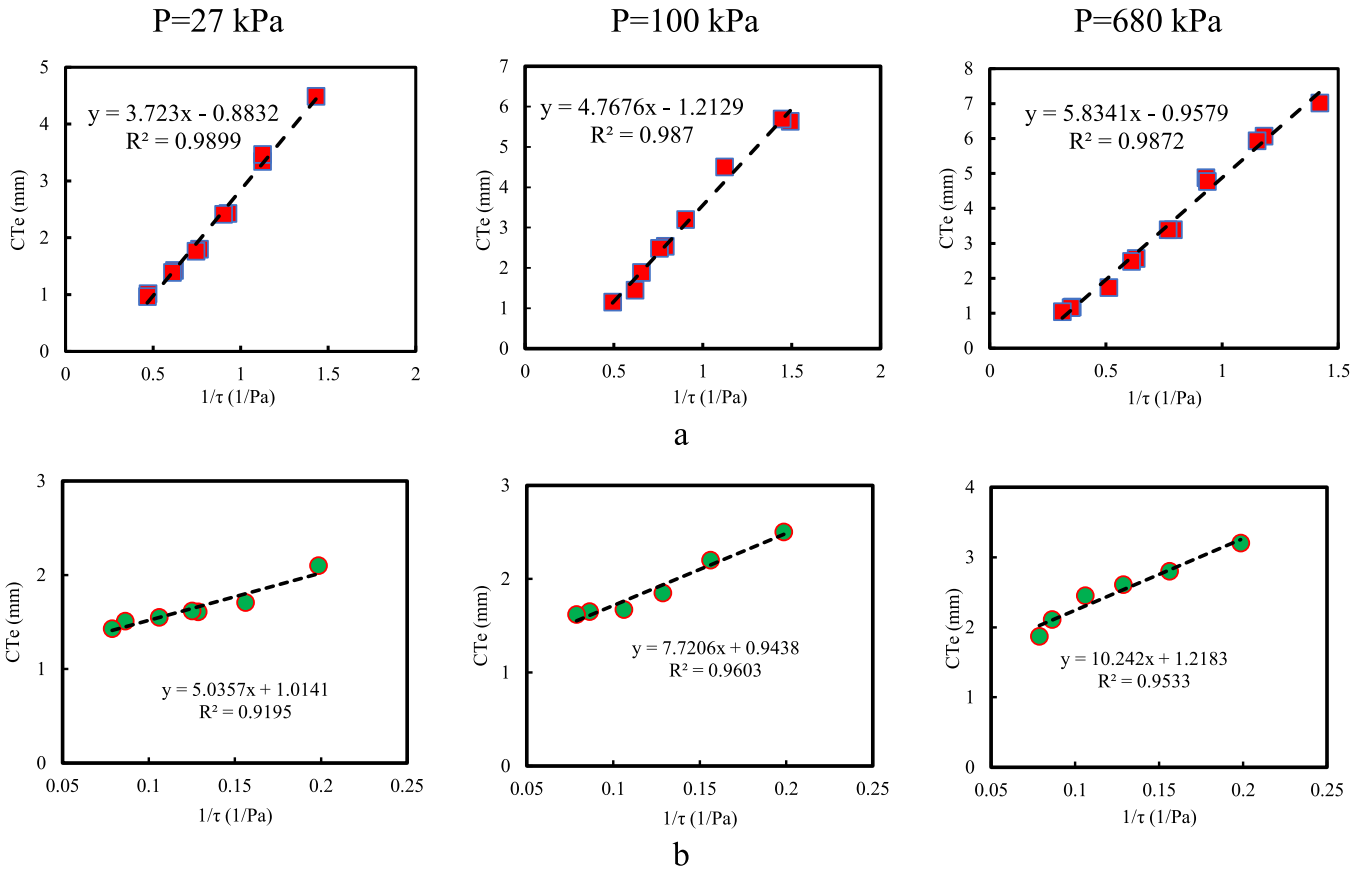

Figure 21. Linear relationship between the cake thickness and inverse of WSS at different pressures for saline mud sample (a) and saline mud sample treated by 1%wt PAM-S (b).

Figure 18 shows the comparison between CFD simulation and experimental results of the mixing time for different rotation speeds. As is shown, there is a good agreement between simulation and experimental results.

Figure 19 shows the CFD results of WSS distribution at different disk rotation speeds for fluids containing saline drilling fluid (1 wt % $CaCl_2$) with a viscosity of 1.4 cp. As can be seen, the WSS is smoothly distributed at low rotational speeds. Respectively, with increasing rotational speed, the WSS distribution changes unevenly because of the creation of vortex flow. Figure 20 shows the effect of different WSS patterns on the mud cake profile. As can be seen, the cake profile proves how to apply shear stress. To model the variation in the cake thickness with WSS, the minimum thickness of the mud cake is equivalent to the area with applying maximum shear stress. Therefore, the minimum cake thickness value corresponds to the maximum WSS for each given rpm.

The dynamic filtration of a saline drilling mud containing 10 wt % bentonite and 1 wt % $CaCl_2$ has been studied as the base test. Figure 21a shows the variation of equilibrium cake thickness (CTe) with WSS at different working pressures. The equilibrium cake thickness means that the cake thickness has been stabilized under specific shear flow and does not change with time. As can be seen, a linear relationship between CTe and $1/\tau$ has been observed, which proves eq 6 under equilibrium conditions. Moreover, as overburden pressure increases, the slope of the fitted line increases, which means that due to the higher filtration flux, a higher WSS needs to avoid cake formation. By adding 1 wt % PAM-S to the base fluid, the effect of the NC on the cake thickness was evaluated under dynamic conditions (Figure 21b). As is shown, the erodibility of the cake layer was decreased due to the increase of the interparticle cohesion, meaning that for removing a specific percentage of cake thickness, a higher WSS is required.

The variation of filtrate flux and volume at the different rotating speeds for saline mud sample are shown in Figure 22a. As can be seen, the filtrate flux increases with rotating speeds meaning the reduction in cake thickness. However, the filtrate flux has not reached a constant value after 30 min, meaning that mud cake also grows over time under dynamic conditions. The results show that increasing the rotating speeds increases the flux rate. Moreover, the variation of cumulative filtrate volume shows a significant difference between static and dynamic conditions. The corresponding linear function of the cumulative filtrate volume has been plotted at each rotating speed, and the minimum error was obtained for the case of 700 rpm (R^2 = 0.9926). As mentioned earlier, based on eq 1, due to the cake growth rate, the filtration volume is a linear function of the square root of time, and only for the constant thickness of the mud cake, the filtrate volume can be described by a linear function of time. Therefore, increasing the shear flow due to the rotation prevents the particles from settling and forming the filter cake, which increases the flux rate. Also, because of the presence of a thin cake at the beginning of filtration, the flux rate is higher than the shear flow velocity leading to the formation of mud cake in the early times. Figure 22b shows the cumulative filtrate volume for the saline mud sample containing NC under shear flow at 700 rpm. As is shown, adding 1 and 2 wt % of NC could reduce the total filtrate loss up to 40 and 68%, respectively. The results indicate that the NC could be more attached to the

https://doi.org/10.1021/acsomega.2c05688
ACS Omega 2022, 7, 44223−44240

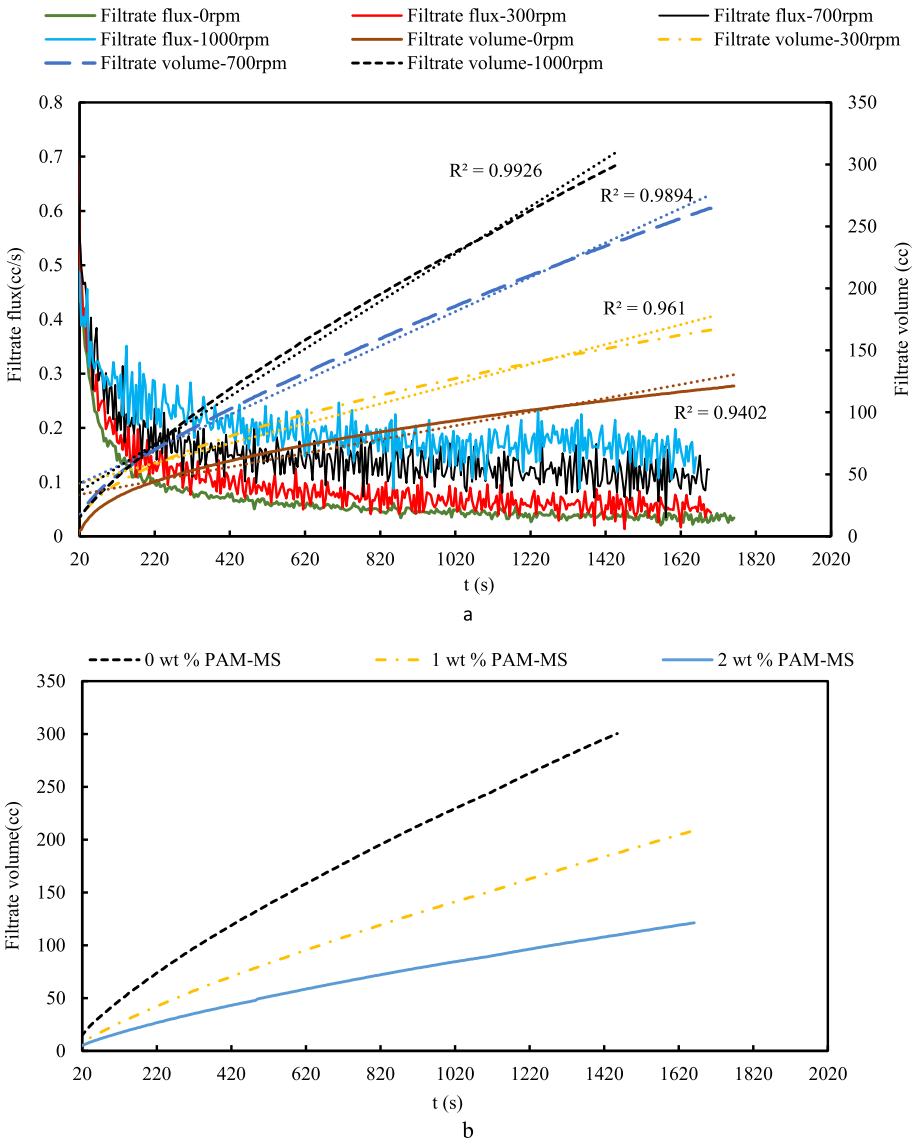

Figure 22. Variation of filtrate flux and volume under dynamic conditions (a), and cumulative filtrate volume for the saline mud sample containing NCs under dynamic conditions (b).

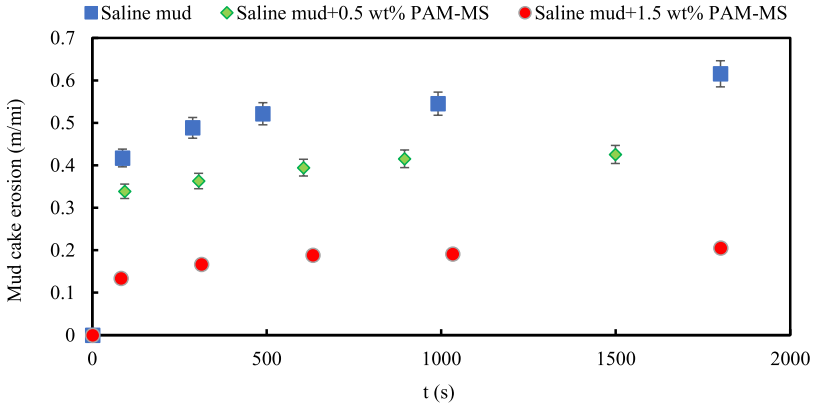

Figure 23. Mud cake erosion for different fluid samples containing NCs at 1000 rpm.

cake surface and create a less permeable and thin mud cake during dynamic filtration.

The variation of predeposited cake thicknesses due to changes in the flow rate inside the wellbore, which may cause a change in the total fluid loss is also crucial. The erosion of the predeposited cake depends on the interface phenomena between the fluid and the cake surface. The higher surface roughness and low interparticle adhesion increase the erodibility of the mud cake,

https://doi.org/10.1021/acsomega.2c05688
ACS Omega 2022, 7, 44223−44240

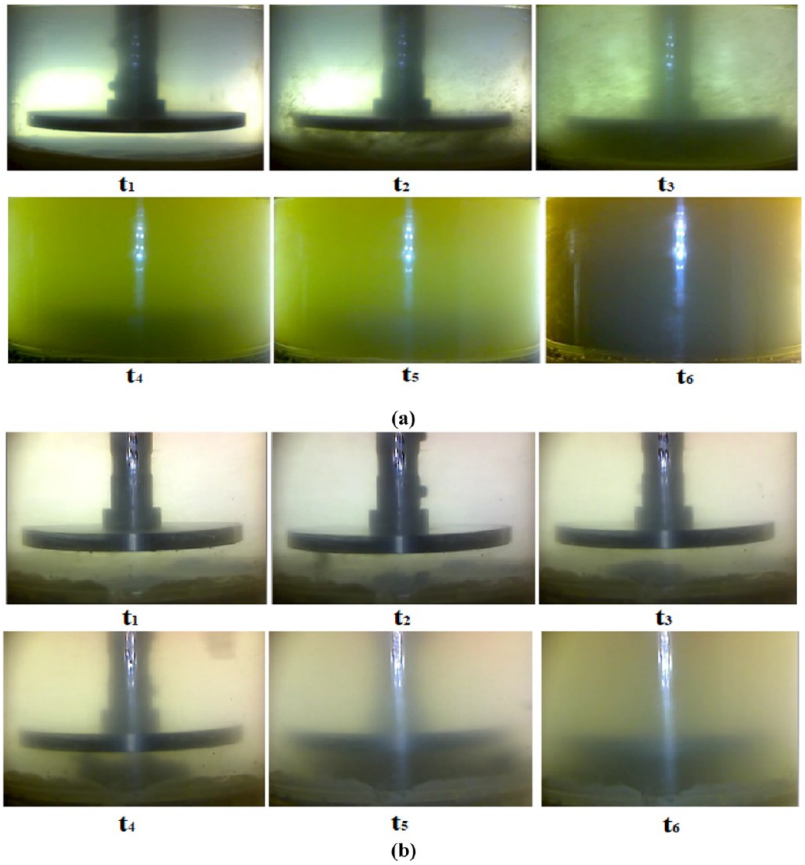

Figure 24. Predeposited cake erosion with time under a fixed shear rate at a disk rotation speed of 300 rpm for the saline mud sample (a) and saline mud sample modified by the NC (b).

while a smooth cake has low erodibility. To investigate the predeposited cake erosion, static filtration was performed, and a mud cake with uniform thickness was created after 30 min. Afterward, the disk started rotating in the filtration cell filled with water, and the mud cake was eroded due to the different imposed WSS on the surface of the cake. The erosion is defined based on the ratio of mud cake weight to initial weight $(\frac{m}{m_i})$.

Figure 23 shows the variation of cake erosion with time at a rotation speed of 1000 rpm. As shown, more than 60% of mud cake was eroded after 30 min for the saline mud sample. Moreover, for mud samples containing PAM-S, the cake erosion is considerably reduced and reaches to 20% at 1.5 wt % PAM-S concentration.

Figure 24 shows the erosion of the predeposited cake layer under a fixed shear flow for both the saline mud sample and saline mud treated by 1 wt % NC at a rotation speed of 300 rpm. As can be seen, erosion is quite time-dependent as the turbidity of fluid increases with time. Moreover, by comparing the turbidity for two samples simultaneously, the mud cake formed from the drilling fluid modified by the NC has a higher resistance against erosion.

4. CONCLUSIONS

In the current study, the effects of nanosilica and the PAM-S NC on improving the rheology and filtration properties of WBDM have been investigated. The NC was synthesized and characterized by FTIR, SEM, and DLS analyses. The filtration rate, mud cake thickness, and SEM images of the mud cake surface were analyzed to verify the enhancement in properties of WBDM containing nanoadditives. Static filtration tests have been conducted under LPLT and HPHT conditions. To investigate the hydrodynamic and formation of a filter cake under shear flow conditions, the dynamic filtration has been conducted in a filtration cell equipped with an agitating system with a disk-type impeller. WSS distribution over the filter cake were analyzed using a 3D CFD technique. The static filtration and dynamic filtration have been also investigated for saline bentonite-WBDM. The following conclusions can be obtained from this study:

- Reduction of permeability occurred by occlusion of microcavities on the surface of the mud cake due to the addition of the NC to WBDM.
- The developed NC can control drilling mud rheology and filtration at low concentrations.
- The effect of silica NPs at low concentrations on both fluid loss and viscosity of WBDM was not favorable.
- Silica NPs at low concentrations reduced the YP of drilling fluid, while NC could control fluid loss and mud cake thickness at low concentrations.
- Rheological properties of WBDM, such as YP, could be affected by bentonite dispersion in the presence of salt, resulting in poor filtration properties.
- The use of an NC at the higher concentration showed that it could reduce the total fluid loss by more than 70% at the 1 wt % concentration.
- In the high-salinity media, the reduction of 60% in the total fluid loss was achieved by adding 1.5 wt % of NC.
- The NC could considerably reduce the cake erosion to 20% at 1.5 wt %.

https://doi.org/10.1021/acsomega.2c05688
ACS Omega 2022, 7, 44223−44240

- Under dynamic conditions, adding 1 and 2 wt % of NC could reduce the total filtrate loss up to 40 and 68%, respectively.

AUTHOR INFORMATION

Corresponding Author

Saeid Jamshidi − *Department of Chemical and Petroleum Engineering, Sharif University of Technology, Tehran 11365-11155, Iran;* orcid.org/0000-0002-6981-1309; Email: jamshidi@sharif.edu

Authors

Hamed Movahedi − *Department of Chemical and Petroleum Engineering, Sharif University of Technology, Tehran 11365-11155, Iran;* orcid.org/0000-0003-2572-6513

Mastaneh Hajipour − *Department of Petroleum Engineering, Science and Research Branch, Islamic Azad University, Tehran 14778-93855, Iran*

Complete contact information is available at: https://pubs.acs.org/10.1021/acsomega.2c05688

Notes

The authors declare no competing financial interest.

ABBREVIATIONS

WBDM: water-based drilling mud
OBDM: oil-based drilling mud
CFD: computational fluid dynamic
PAM-S: polyacrylamide-silica
NPs: nanoparticles
NC: nanocomposite
FTIR: Fourier transform infrared spectroscopy
SEM: scanning electron microscopy
DLS: dynamic light scattering
LPLT: low pressure-low temperature
HPHT: high pressure-high temperature

REFERENCES

(1) Caenn, R.; Chillingar, G. V. Drilling fluids: State of the art. *J. Pet. Sci. Eng.* **1996**, *14*, 221−230.
(2) Movahedi, H.; Jamshidi, S. Experimental and CFD simulation of slurry flow in the annular flow path using two-fluid model. *J. Pet. Sci. Eng.* **2021**, *198*, No. 108224.
(3) Hajipour, M. CFD simulation of turbulent flow of drill cuttings and parametric studies in a horizontal annulus. *SN Appl. Sci.* **2020**, *2*, 1146.
(4) Movahedi, H.; Shad, S.; Mokhtari-Hosseini, Z. B. Modeling and simulation of barite deposition in an annulus space of a well using CFD. *J. Pet. Sci. Eng.* **2018**, *161*, 476−496.
(5) Moghaddam, A. K.; Saadatabadi, A. R. Mesoscopic rheological modeling of drilling fluids: Effects of the electrolyte. *J. Pet. Sci. Eng.* **2020**, *195*, No. 107880.
(6) JIANG, G.; He, S.; Yinbo, H. The biodiesel-based flat-rheology drilling fluid system. *Pet. Explor. Dev.* **2022**, *49*, 200−210.
(7) Cheng, R.; Lei, Z.; Bai, Y.; Zhang, J.; Hao, H.; Xie, G. Preparation of the Tetrameric Poly (VS-St-BMA-BA) Nano-Plugging Agent and Its Plugging Mechanism in Water-Based Drilling Fluids. *ACS Omega* **2022**, *7*, 28304−28312.
(8) Bageri, B. S.; Gamal, H.; Elkatatny, S.; Patil, S. Effect of different weighting agents on drilling fluids and filter cake properties in sandstone formations. *ACS Omega* **2021**, *6*, 16176−16186.
(9) Fanhui, Z.; Zhang, Q.; Jianchun, G.; Bo, Z.; Zhang, Y.; Songgen, H. Mechanisms of shale hydration and water block removal. *Pet. Explor. Dev.* **2021**, *48*, 752−761.
(10) Zhou, G.; Qiu, Z.; Zhong, H.; Zhao, X.; Kong, X. Study of environmentally friendly wild Jujube pit powder as a water-based drilling fluid additive. *ACS Omega* **2021**, *6*, 1436−1444.
(11) Movahedi, H.; Farahani, M. V.; Jamshidi, S. Application of Hydrated Basil Seeds (HBS) as the herbal fiber on hole cleaning and filtration control. *J. Pet. Sci. Eng.* **2017**, *152*, 212−228.
(12) Salehi, S.; Madani, S. A.; Kiran, R. Characterization of drilling fluids filtration through integrated laboratory experiments and CFD modeling. *J. Nat. Gas Sci. Eng.* **2016**, *29*, 462−468.
(13) Kalantariasl, A.; Bedrikovetsky, P. Stabilization of external filter cake by colloidal forces in a "well−reservoir" system. *Ind. Eng. Chem. Res.* **2014**, *53*, 930−944.
(14) Kalantariasl, A.; Farajzadeh, R.; You, Z.; Bedrikovetsky, P. Nonuniform external filter cake in long injection wells. *Ind. Eng. Chem. Res.* **2015**, *54*, 3051−3061.
(15) Ibrahim, M. A.; Saleh, T. A. Synthesis of efficient stable dendrimer-modified carbon for cleaner drilling shale inhibition. *J. Environ. Chem. Eng.* **2021**, *9*, No. 104792.
(16) JIANG, G.; Xiaoxiao, N.; Wuquan, L.; Xiaohu, Q.; Xuwu, L. Super-amphiphobic, strong self-cleaning and high-efficiency water-based drilling fluids. *Pet. Explor. Dev.* **2020**, *47*, 421−429.
(17) Saleh, T. A.*Nanotechnology in oil and gas industries*; Springer: Cham, Switzerland, 2018; pp 145−160.
(18) Saleh, T. A.; Ibrahim, M. A. Advances in functionalized Nanoparticles based drilling inhibitors for oil production. *Energy Rep.* **2019**, *5*, 1293−1304.
(19) Cheraghi, M.; Hajipour, M.; Emamzadeh, A. Enhancement of the heat capacity of water-based drilling fluids for deep drilling applications. *Braz. J. Chem. Eng.* **2022**, *39*, 77−86.
(20) Al-Shargabi, M.; Davoodi, S.; Wood, D. A.; Al-Musai, A.; Rukavishnikov, V. S.; Minaev, K. M. Nanoparticle applications as beneficial oil and gas drilling fluid additives: A review. *J. Mol. Liq.* **2022**, *352*, No. 118725.
(21) Davoodi, S.; Al-Shargabi, M.; Wood, D. A.; Rukavishnikov, V. S.; Minaev, K. M. Experimental and field applications of nanotechnology for enhanced oil recovery purposes: A review. *Fuel* **2022**, *324*, No. 124669.
(22) Deng, S.; Huang, Y.; Hu, X.; Wang, H.; Zhao, H.; He, J. Nano-Film-Forming Plugging Drilling Fluid and Bridging Cross-Linking Plugging Agent Are Used to Strengthen Wellbores in Complex Formations. *ACS Omega* **2022**, *7*, 22804−22810.
(23) Veisi, E.; Hajipour, M.; Delijani, E. B. Experimental study on thermal, rheological and filtration control characteristics of drilling fluids: effect of nanoadditives. *Oil Gas Sci. Technol. − Rev. IFP Energies nouvelle* **2020**, 36.
(24) Li, M.-C.; Wu, Q.; Han, J.; Mei, C.; Lei, T.; Lee, S.-Y.; Gwon, J. Overcoming salt contamination of bentonite water-based drilling fluids with blended dual-functionalized cellulose nanocrystals. *ACS Sustainable Chem. Eng.* **2020**, *8*, 11569−11578.
(25) Aftab, A.; Ali, M.; Sahito, M. F.; Mohanty, U. S.; Jha, N. K.; Akhondzadeh, H.; Azhar, M. R.; Ismail, A. R.; Keshavarz, A.; Iglauer, S. Environmental friendliness and high performance of multifunctional tween 80/ZnO-nanoparticles-added water-based drilling fluid: an experimental approach. *ACS Sustainable Chem. Eng.* **2020**, *8*, 11224−11243.
(26) Jinsheng, S.; Yingrui, B.; Cheng, R.; Kaihe, L.; Fan, L.; Jie, F.; Shaofei, L.; ZHANG, J.; Huijun, H. Research progress and prospect of plugging technologies for fractured formation with severe lost circulation. *Pet. Explor. Dev.* **2021**, *48*, 732−743.
(27) Alvi, M. A. A.; Belayneh, M.; Fjelde, K. K.; Saasen, A.; Bandyopadhyay, S. Effect of Hydrophobic Iron Oxide Nanoparticles on the Properties of Oil-Based Drilling Fluid. *J. Energy Resour. Technol.* **2021**, *143*, No. 043001.
(28) Bayat, A. E.; Harati, S.; Kolivandi, H. Evaluation of rheological and filtration properties of a polymeric water-based drilling mud in presence of nano additives at various temperatures. *Colloids Surf., A* **2021**, *627*, No. 127128.
(29) Vryzas, Z.; Kelessidis, V. C. Nano-based drilling fluids: A review. *Energies* **2017**, *10*, 540.

(30) Abdo, J.; Haneef, M. Clay nanoparticles modified drilling fluids for drilling of deep hydrocarbon wells. *Appl. Clay Sci.* **2013**, *86*, 76−82.
(31) Afolabi, R. O.; Orodu, O. D.; Seteyeobot, I. Predictive modelling of the impact of silica nanoparticles on fluid loss of water based drilling mud. *Appl. Clay Sci.* **2018**, *151*, 37−45.
(32) Mohamed, A.; Salehi, S.; Ahmed, R.; Li, G. Experimental study on rheological and settling properties of shape memory polymer for fracture sealing in geothermal formations. *J. Pet. Sci. Eng.* **2022**, *208*, No. 109535.
(33) Zhong, H.; Kong, X.; Chen, S.; Grady, B. P.; Qiu, Z. Preparation, characterization and filtration control properties of crosslinked starch nanospheres in water-based drilling fluids. *J. Mol. Liq.* **2021**, *325*, No. 115221.
(34) Lei, M.; Huang, W.; Sun, J.; Shao, Z.; Duan, W.; Wu, T.; Wang, Y. Synthesis, characterization, and performance of carboxymethyl chitosan with different molecular weight as additive in water-based drilling fluid. *J. Mol. Liq.* **2020**, *310*, No. 113135.
(35) Li, X.; Jiang, G.; Shen, X.; Li, G. Application of tea polyphenols as a biodegradable fluid loss additive and study of the filtration mechanism. *ACS Omega* **2020**, *5*, 3453−3461.
(36) Shan, W.; Ma, J.; Jiang, G.; Sun, J.; An, Y. An Inverse Emulsion Polymer as a Highly Effective Salt-and Calcium-Resistant Fluid Loss Reducer in Water-Based Drilling Fluids. *ACS Omega* **2022**, 16141.
(37) Moghaddam, A. K.; Saadatabadi, A. R. Rheological modeling of water based drilling fluids containing polymer/bentonite using generalized bracket formalism. *J. Pet. Sci. Eng.* **2020**, *189*, No. 107028.
(38) Movahedi, H.; Jamshidi, S.; Hajipour, M. New insight into the filtration control of drilling fluids using a graphene-based nanocomposite under static and dynamic conditions. *ACS Sustainable Chem. Eng.* **2021**, *9*, 12844−12857.
(39) Ibrahim, M. A.; Saleh, T. A. Partially aminated acrylic acid grafted activated carbon as inexpensive shale hydration inhibitor. *Carbohydr. Res.* **2020**, *491*, No. 107960.
(40) Rana, A.; Arfaj, M. K.; Saleh, T. A. Graphene grafted with glucopyranose as a shale swelling inhibitor in water-based drilling mud. *Appl. Clay Sci.* **2020**, *199*, No. 105806.
(41) Ma, J.; Pang, S.; Zhang, Z.; Xia, B.; An, Y. Experimental study on the polymer/graphene oxide composite as a fluid loss agent for water-based drilling fluids. *ACS Omega* **2021**, *6*, 9750−9763.
(42) Mao, H.; Qiu, Z.; Shen, Z.; Huang, W. Hydrophobic associated polymer based silica nanoparticles composite with core−shell structure as a filtrate reducer for drilling fluid at utra-high temperature. *J. Pet. Sci. Eng.* **2015**, *129*, 1−14.
(43) An, Y.; Jiang, G.; Qi, Y.; Ge, Q.; Zhang, L. Nano-fluid loss agent based on an acrylamide based copolymer "grafted" on a modified silica surface. *RSC Adv.* **2016**, *6*, 17246−17255.
(44) Kamali, F.; Saboori, R.; Sabbaghi, S. Fe3O4-CMC nanocomposite performance evaluation as rheology modifier and fluid loss control characteristic additives in water-based drilling fluid. *J. Pet. Sci. Eng.* **2021**, *205*, No. 108912.
(45) Movahedi, H.; Jamshidi, S. New insight into hydrodynamic and cake erosion mechanism during rotating-disk dynamic microfiltration of concentrated bentonite suspensions at different salinity conditions. *Sep. Purif. Technol.* **2022**, *300*, No. 121844.
(46) Bourgoyne, A. T.; Millheim, K. K.; Chenevert, M. E.; Young, F. S.*Applied drilling engineering*; Society of Petroleum Engineers Richardson: TX, 1986; Vol. 2, pp 42 −81.
(47) Tyagi, B.; Chudasama, C. D.; Jasra, R. V. Determination of structural modification in acid activated montmorillonite clay by FT-IR spectroscopy. *Spectrochim. Acta, Part A* **2006**, *64*, 273−278.
(48) Arjmandi, M.; Ramezani, M. Mechanical and tribological assessment of silica nanoparticle-alginate-polyacrylamide nanocomposite hydrogels as a cartilage replacement. *J. Mech. Behav. Biomed. Mater.* **2019**, *95*, 196−204.
(49) Corredor, L. M.; Husein, M. M.; Maini, B. B. Impact of PAM-grafted nanoparticles on the performance of hydrolyzed polyacrylamide solutions for heavy oil recovery at different salinities. *Ind. Eng. Chem. Res.* **2019**, *58*, 9888−9899.
(50) Zhuang, G.; Zhang, Z.; Jaber, M. Organoclays used as colloidal and rheological additives in oil-based drilling fluids: An overview. *Appl. Clay Sci.* **2019**, *177*, 63−81.
(51) Lei, M.; Huang, W.; Sun, J.; Shao, Z.; Wu, T.; Liu, J.; Fan, Y. Synthesis of carboxymethyl chitosan as an eco-friendly amphoteric shale inhibitor in water-based drilling fluid and an assessment of its inhibition mechanism. *Appl. Clay Sci.* **2020**, *193*, No. 105637.
(52) Li, G.; Zhao, Z.; Liu, J.; Jiang, G. Effective heavy metal removal from aqueous systems by thiol functionalized magnetic mesoporous silica. *J. Hazard. Mater.* **2011**, *192*, 277−283.
(53) Showkat, A. M.; Zhang, Y.-P.; Kim, M.-S.; Gopalan, A. I.; Reddy, K. R.; Lee, K.-P. Analysis of heavy metal toxic ions by adsorption onto amino-functionalized ordered mesoporous silica. *Bull. Korean Chem. Soc.* **2007**, *28*, 1985−1992.
(54) Varlot, K.; Reynaud, E.; Kloppfer, M.; Vigier, G.; Varlet, J. Clay-reinforced polyamide: Preferential orientation of the montmorillonite sheets and the polyamide crystalline lamellae. *J. Polym. Sci., Part B: Polym. Phys.* **2001**, *39*, 1360−1370.
(55) Movahedi, H.; Vasheghani Farahani, M.; Masihi, M. Development of a Numerical Model for Single-and Two-Phase Flow Simulation in Perforated Porous Media. *J. Energy Resour. Technol.* **2020**, *142*, No. 042901.

https://doi.org/10.1021/acsomega.2c05688
ACS Omega 2022, 7, 44223−44240